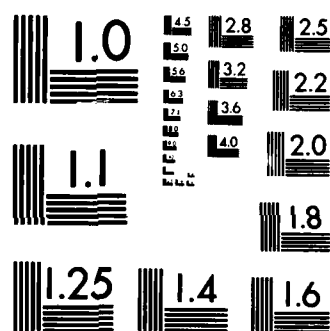END

FILMED

DTIC

MICROCOPY RESOLUTION TEST CHART

NATIONAL BUREAU OF STANDARDS-1963-A

AFATL-TR-82-9

Loading on Penetrators in Concrete Slabs

John J Osborn

ORLANDO TECHNOLOGY, INC
P O BOX 855
SHALIMAR, FLORIDA 32579

FEBRUARY 1982

FINAL REPORT FOR PERIOD MAY 1981-SEPTEMBER 1981

AD A121142

DTIC FILE COPY

Air Force Armament Laboratory
AIR FORCE SYSTEMS COMMAND ★ UNITED STATES AIR FORCE ★ EGLIN AIR FORCE BASE, FLORIDA

82 11 05 045

NOTICE

Please do not request copies of this report from the Air Force Armament Laboratory. Additional copies may be purchased from:

National Technical Information Service
5285 Port Royal Road
Springfield, Virginia 22161

Federal Government agencies and their contractors registered with Defense Technical Information Center should direct requests for copies of this report to:

Defense Technical Information Center
Cameron Station
Alexandria, Virginia 22314

REPORT DOCUMENTATION PAGE		READ INSTRUCTIONS BEFORE COMPLETING FORM
1. REPORT NUMBER AFATL-TR-82-9	2. GOVT ACCESSION NO. *A121 142*	3. RECIPIENT'S CATALOG NUMBER
4. TITLE *(and Subtitle)* LOADING ON PENETRATORS IN CONCRETE SLABS		5 TYPE OF REPORT & PERIOD COVERED Final Report 1 May – 30 September 1981
		6. PERFORMING ORG. REPORT NUMBER
7. AUTHOR(s) John J. Osborn		8. CONTRACT OR GRANT NUMBER(s) F08635-81-C-0050
9. PERFORMING ORGANIZATION NAME AND ADDRESS Orlando Technology, Incorporated P.O. Box 855 Shalimar, Florida 32579		10. PROGRAM ELEMENT, PROJECT, TASK AREA & WORK UNIT NUMBERS PE: 62602F JON: 2543-19-24
11. CONTROLLING OFFICE NAME AND ADDRESS Air Force Armament Laboratory /DLYV Armament Division Eglin Air Force Base, FL 32542		12. REPORT DATE February 1982
		13 NUMBER OF PAGES 66
14. MONITORING AGENCY NAME & ADDRESS*(if different from Controlling Office)*		15. SECURITY CLASS. *(of this report)* Unclassified
		15a. DECLASSIFICATION DOWNGRADING SCHEDULE

16. DISTRIBUTION STATEMENT *(of this Report)*

Approved for public release; distribution unlimited.

17. DISTRIBUTION STATEMENT *(of the abstract entered in Block 20, if different from Report)*

18. SUPPLEMENTARY NOTES

Availability of this report is specified on verso of front cover.

19. KEY WORDS *(Continue on reverse side if necessary and identify by block number)*

Concrete
Penetration
Model
Loading
Saturated Concrete

20 ABSTRACT *(Continue on reverse side if necessary and identify by block number)*

This report presents hydrocode calculations and a model describing them for penetrations of finite thickness concrete slabs by steel penetrators travelling at 100 to 500 m/s. The report also discusses the effects of saturation on loading on penetrators.
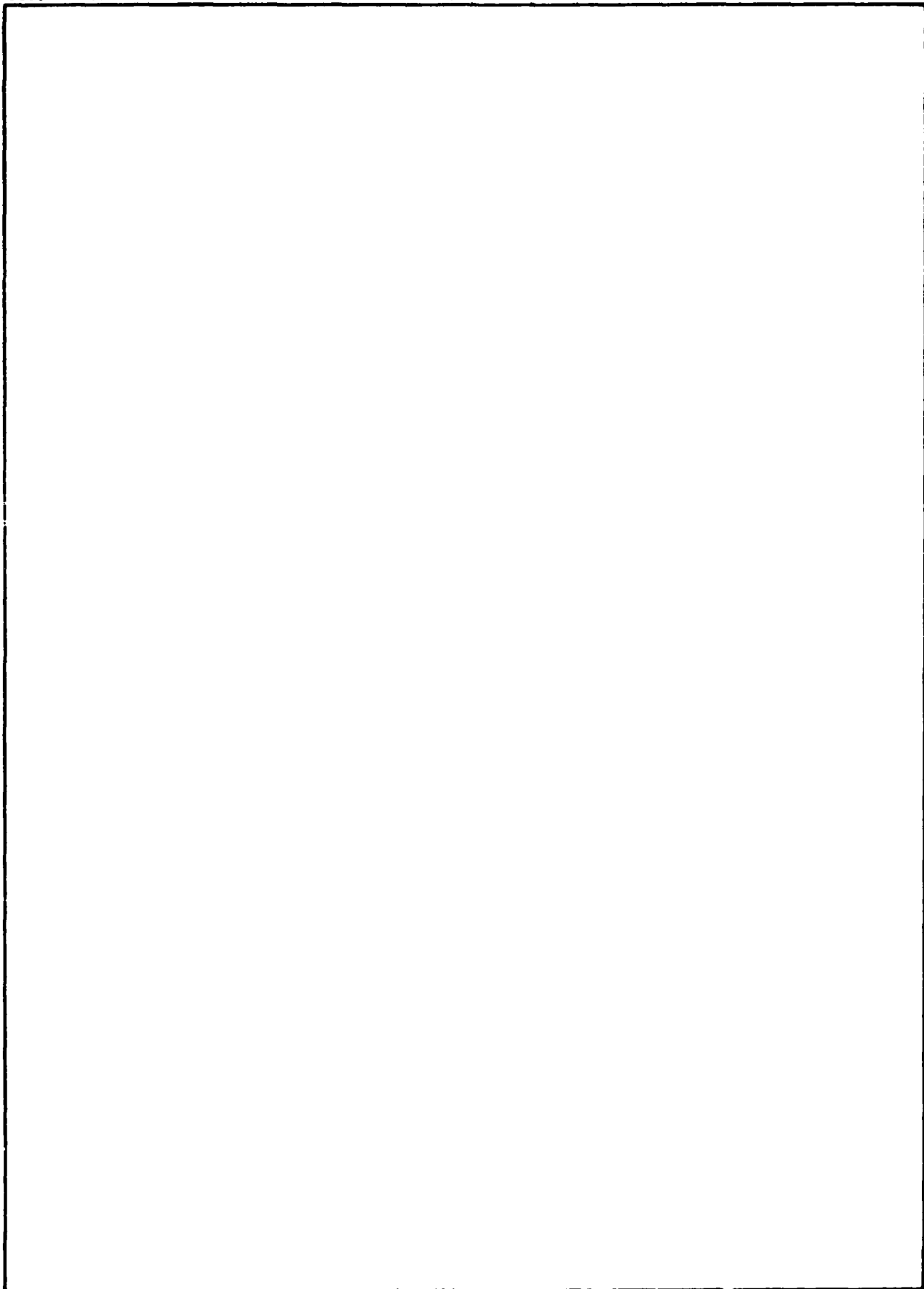
PREFACE

The calculations and analyses contained in this report were performed by Orlando Technology, Incorporated, P.O. Box 855, Shalimar, Florida, under subcontract to Datatec, Inc., 182 Green Acres Road, Fort Walton Beach, Florida. The basic contract between the Air Force Armament Laboratory and Datatec, Inc. is F08635-81-C-0050. Work in this report was performed under Task Directive 3 of that contract. The work was performed by Mr. John Osborn. Mr. John Collins was the program manager for the Armament Laboratory.

The public affairs office has reviewed this report, and it is releasable to the National Technical Information Service (NTIS), where it will be available to the general public, including foreign nationals.

This technical report has been reviewed and is approved for publication.

FOR THE COMMANDER

JAMES L. THOREEN
Chief, Analysis Division

(The reverse of this page is blank)

TABLE OF CONTENTS

LIST OF FIGURES

LIST OF SYMBOLS

A	Hugoniot Coefficient
B	Hugoniot Coefficient
C	Hugoniot Coefficient
c	Sound Speed
D	Projectile or Element Diameter
f_c	Volume Fraction of Concrete
f_{mc}	Mass Fraction of Concrete
f_w	Volume Fraction of Water
f_{wc}	Mass Fraction of Water
f'_c	Unconfined Compressive Strength
P	Pressure
R	Radius
s	Shock Velocity/Particle Velocity Slope
t	Time
T	Concrete Thickness
v	Volume
V	Velocity
Y	Yield Strength
ρ	Density
μ	Excess Compression
τ	Stress

SECTION I
SUMMARY

The purpose of this Task Directive was to investigate and model loading on a projectile impacting air- or sand-backed concrete slabs of finite thickness. The model developed can be used to predict loads on a projectile impacting these media if the impact is at normal incidence. It can be used to predict total forces on the projectile or it can be used to predict forces on projectile elements if the projectile's trajectory is run in a terradynamics code.

A number of calculations were performed using various projectile geometries and velocities in a finite difference wave propagation computer program (hydrocode). Loads on the projectile were saved and analyzed to develop equations for predicting applied stress versus time as functions of the projectile's geometry and velocity and the thickness of the concrete target. These loading equations are presented in this report.

In addition, loads on a projectile impacting a completely saturated concrete were investigated using a saturated concrete model developed by the Sandia National Laboratories. This investigation was performed because there was some Air Force interest in a comparison of loads for saturated and dry concrete.

SECTION II

MATERIAL PROPERTIES

A word concerning units is in order before proceeding into a discussion concerning material properties. The hydrocodes in use at Orlando Technology, Inc. (OTI) employ the centimeter-gram-second (CGS) system of units. This is a convenient system of units for conventional weapon problems with the exception that pressure can be a very large number (10^9 dynes/cm^2) for the problems of interest in this report. Prior to general acceptance of the Systeme International d'Unites (SI) system, kilobars (1 kilobar = 10^9 dynes/cm^2) were used to reduce these large pressures to manageable numbers. Because previous work (Reference 1) employed kilobars, this unit has been retained in this report. For SI users, 1 Gigapascal is equal to 10 kilobars. The units of psi (pounds per square inch) are used only in reference to the unconfined compressive strength of a concrete, in line with a very old tradition.

The dry concrete material behavior model used in all hydrocode runs is presented in detail in Reference 2. The model consists of a hydrostat and a yield surface. These curves are seen in Figure 1. The hydrostat defines a relationship between pressure and density and is valid for a good quality concrete with an unconfined compressive strength of 5,000 psi. The hydrostat loading curves, up to 60 kilobars (Kb) are defined by the following equations:

$$P(Kb) = 144 \ \mu \qquad \qquad \text{if } 0 \leq \mu \leq 0.0025$$

$$P(Kb) = 0.358 + 78.62 \ (\mu - 0.0025) \qquad \text{if } 0.0025 < \mu \leq 0.1$$

$$P(Kb) = 8.0 + 130.0 \ (\mu - 0.1) \qquad \text{if } 0.1 < \mu \leq 0.2$$

$$P(Kb) = 21.0 + 420.0 \ (\mu - 0.2) \qquad \text{if } 0.2 < \mu \leq 0.3$$

In these equations, P is the pressure (position in compression) and μ is the excess compression defined by:
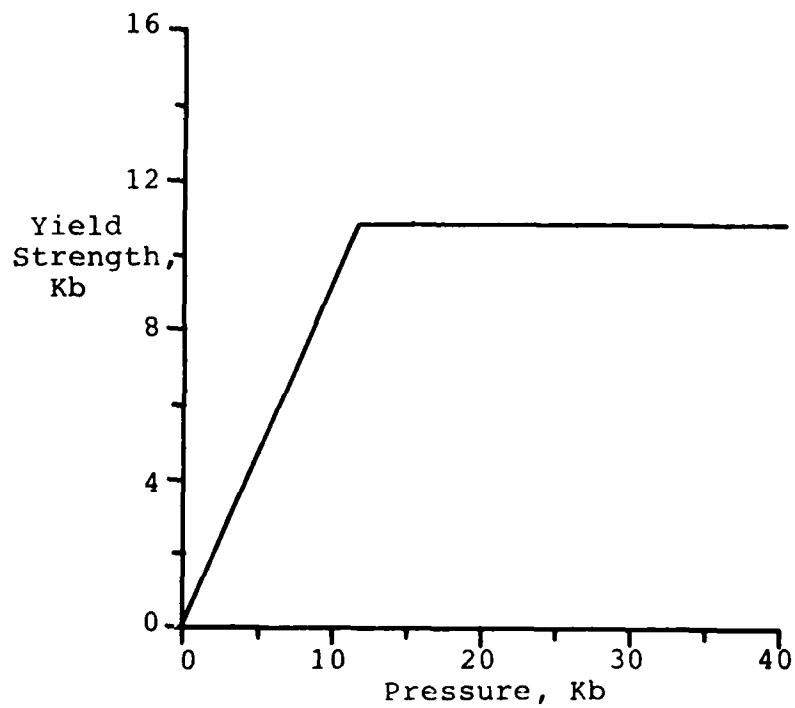
$$\mu = \frac{\rho}{\rho_0} - 1$$
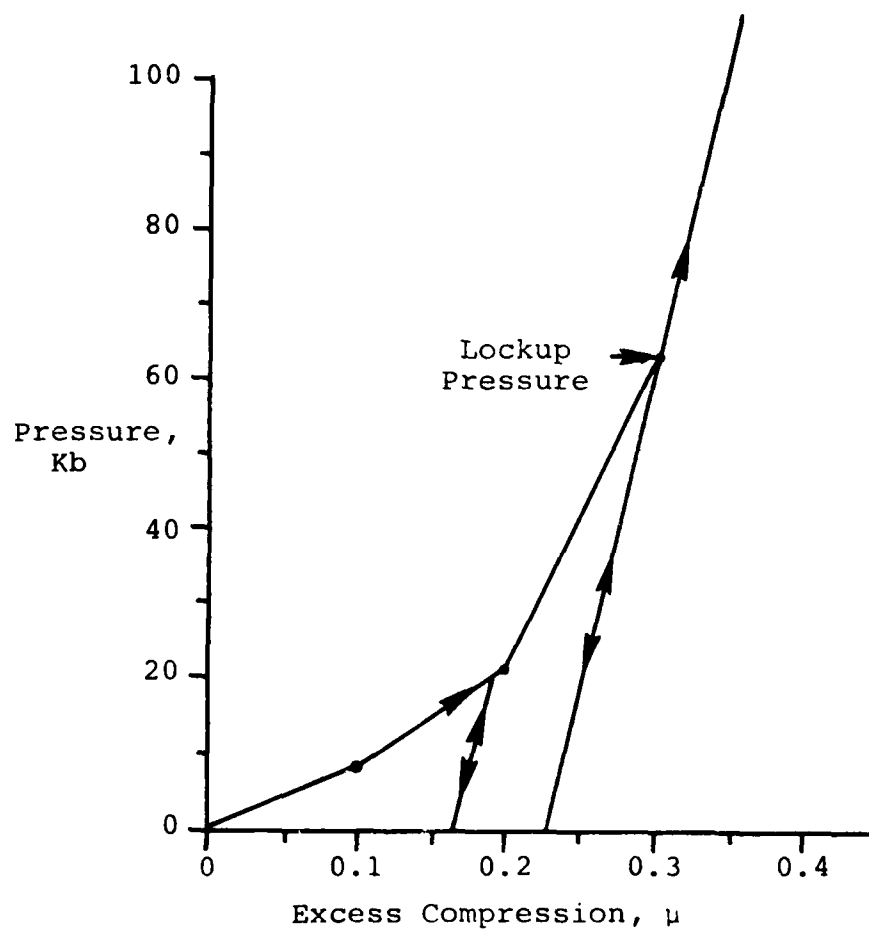
Figure 1. Hydrostat and Yield Surface for 5000 PSI Concrete.

3

where ρ_o is ambient concrete density (2.2 g/cc) and ρ is the density at some compressed state.

Unloading prior to reaching the lockup portion of the hydrostat is along paths parallel to the lockup curve. Reloading is along these same paths. This occurs because the concrete crushes in loading and will occupy less volume when this loading is relieved.

The yield surface was developed from test data for concretes with varying unconfined compressive strengths and is a function of pressure and the unconfined strength. The yield strength is defined by the following equations:

$$Y = 3.3(P + 0.1f_c'/3) \qquad \text{if } -0.1f_c'/3 < P \leq fc_c'/3$$

$$Y = P + 2/3f_c' \qquad \text{if } \frac{f_c'}{3} < P \leq 30f_c'$$

$$Y = 30.67f_c' \qquad \text{if } 30f_c' < P$$

In these equations f_c' is the concrete's unconfined compressive strength. The yield surface is a Mohr-Coulomb type with a saturation level (arbitrarily) set at $30.67f_c'$.

This concrete model has been successfully employed in penetration and breaching calculations and is actively used at the Air Force Armament Laboratory, the Air Force Weapons Laboratory, the Army Ballistic Research Laboratory and other locations.

The wet concrete model is one developed by M. M. Hightower of the Sandia National Laboratories and is presented in detail in Reference 3. Hightower basically proposes that water content can be taken into account by combining the dry concrete and water hydrostats and by reducing the concrete's yield strength. In the ultimate, fully saturated concrete, the material has no yield strength whatsoever. The material model for this fully saturated concrete is discussed below.

4

Let f_c be the volume fraction of concrete and f_w be the volume fraction of water at any time. Initial values, consistent with the void fraction in the OTI dry concrete model, are:

$$f_{co} = 0.818$$
$$f_{wo} = 0.182$$

In this situation all of the void volume is filled with water. Because of the varying compressibilities of concrete and water, f_c and f_w vary if pressure equilibrium between the concrete and water is desired within a zone. Although the volume fractions vary, the mass fractions do not and so:

$$f_{mc} = \rho_{oc} f_{co} / \rho_o$$
$$f_{mw} = \rho_{ow} f_{wo} / \rho_o$$

where

f_{mc} is the mass fraction of concrete

f_{mw} is the mass fraction of water

ρ_{oc} is the initial density of concrete (2.69 gm/cc)

ρ_{ow} is the initial density of water (1.0 gm/cc)

ρ_o is the initial density of the concrete/water mixture.

The value ρ_o is found from

$$\rho_o = \rho_{oc} f_{co} + \rho_{ow} f_{wo} = 2.38 \text{ gm/cc}$$

As the material is compressed f_c and f_w vary but f_{mc} and f_{mw} remain constant, so that:

$$f_{mc} = \frac{m_c}{m} = \frac{\rho_c v_c}{\rho v} = \frac{\rho_c}{\rho} f_c$$

where

m_c is the mass of concrete in a zone

m is the total mass in a zone

v_c is the volume of concrete in a zone

v   is the total volume of a zone

ρ_c is the density of concrete in a zone

ρ is the total density in a zone

The excess compression for a zone, μ, is defined by

$$\mu = \frac{\rho}{\rho_o} - 1$$

The excess compression for the concrete in a zone, μ_c, is defined by

$$\mu_c = \frac{\rho_c}{\rho_{oc}} - 1$$

therefore

$$\rho = \rho_o \, (\mu + 1) \qquad \text{and}$$

$$\rho_c = \rho_{oc} \, (\mu_c + 1)$$

Substitution yields

$$f_{mc} = \frac{\rho_{oc}(\mu_c + 1) f_c}{\rho_o (\mu + 1)}$$

which can be solved for μ_c as a function of μ and f_c

$$\mu_c = \frac{f_{mc}\rho_o(\mu + 1)}{\rho_{oc} f_c} - 1$$

Similarly,

$$\mu_w = \frac{f_{mw}\rho_o(\mu + 1)}{\rho_{ow}(1 - f_c)} - 1$$

where $1 - f_c$ has been substituted for f_w.

It was necessary to be able to define expressions for μ_c and μ_w since pressure
will be expressed in the Hugoniot form

6

$$P = A\mu + B\mu^2 + C\mu^3$$

If shock Hugoniot data is available

$A = \rho_0 c_0^2$

$B = A(1+2(s-1))$

$C = A(2(s-1) + 3(s-1)^2)$

where ρ_0 is initial density, c_0 is initial bulk sound speed and s is the slope of the shock velocity vs particle velocity curve. For water these values are

$\rho_0 = 1.0$

$c_0 = 1.483 \times 10^5$ cm/sec

$s = 1.75$

leading to

$A_w = 22$ Kb

$B_w = 55$ Kb

$C_w = 70$ Kb

The pure concrete hydrostat can be taken from the lockup curve from the dry concrete model. In this model, ambient pressure occurs at a μ value of 0.223 where

$$\mu = \frac{\rho}{2.2} - 1$$

and the pressure is 105.76 Kb at $\mu = 0.36607$ (based again on $\rho_0=2.2$). At this pressure level the derivative of P with respect to μ is 784 Kb. Shifting the curve so that zero pressure occurs at $\mu=0$ (based on $\rho_0=2.69$) means that the pressure level of 105.76 Kb occurs at $\mu=0.143$, as does the derivative value of 784 Kb. Since P will always be zero when μ is zero, these conditions provide only two equations. It was decided to set the C term to zero and solve for A and B. These values are

$A_c = 695$ Kb

$B_c = 311$ Kb

7

The condition of pressure equilibrium then requires that

$$22\mu_w + 55\mu_w^2 + 70\mu_w^3$$
$$= 695\mu_c + 311\mu_c^2$$

The equations for μ_c and μ_w can be substituted into the above equation to provide a single equation for f_c. After iteratively solving it for f_c, f_w can be found from

$$f_w = 1 - f_c$$

allowing one to solve for μ_c and μ_w. Either value of μ can be used in the appropriate pressure equation to determine zone pressure.

Figure 2 is a plot of the combined hydrostats with values of f_c and f_w indicated on the plot. The μ value in the plot is total zone μ. The dry concrete hydrostat is shown on the plot for reference. It can be seen that the sound speed for the saturated concrete will be 2 to 3 times that for the dry concrete up to approximately 30 kb. After this point the two sound speeds will be essentially equal.

Hightower proposes that the wet concrete's yield strength will be a function of the water content and that it is zero when the concrete is fully saturated. Hence, for this fully saturated model there is no yield strength in the material.

The dry sand model used in the calculations presented in this report was developed from two sources. Low pressure hydrostatic data from Reference 4 was combined with high pressure Hugoniot data from Reference 5. The sand has an initial density of 1.6 gm/cc. It is assumed to have no yield strength and is therefore represented only by a hydrostat. The hydrostat is shown in Figure 3.

8
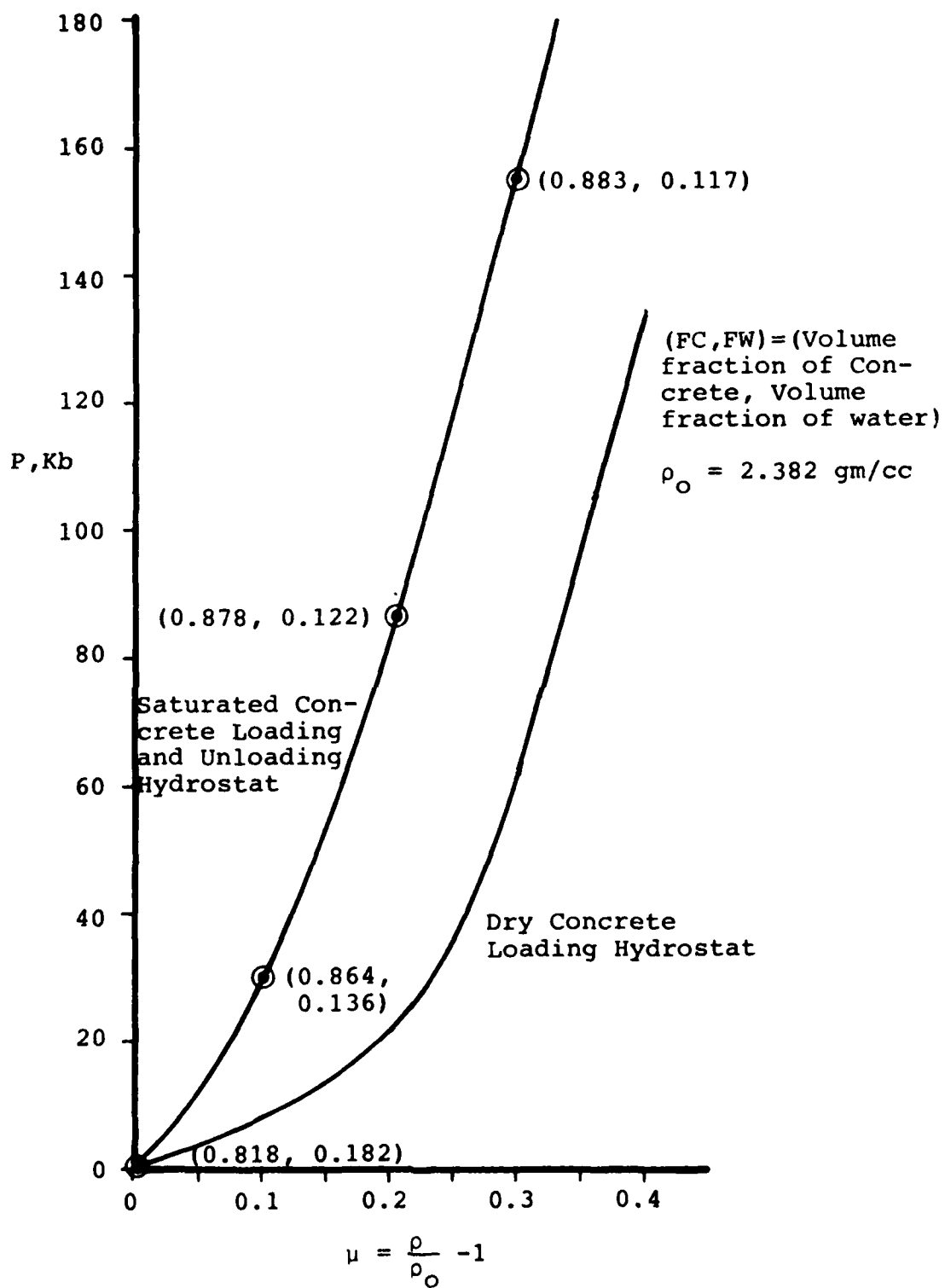
Figure 2.   Saturated Concrete Hydrostat.

9

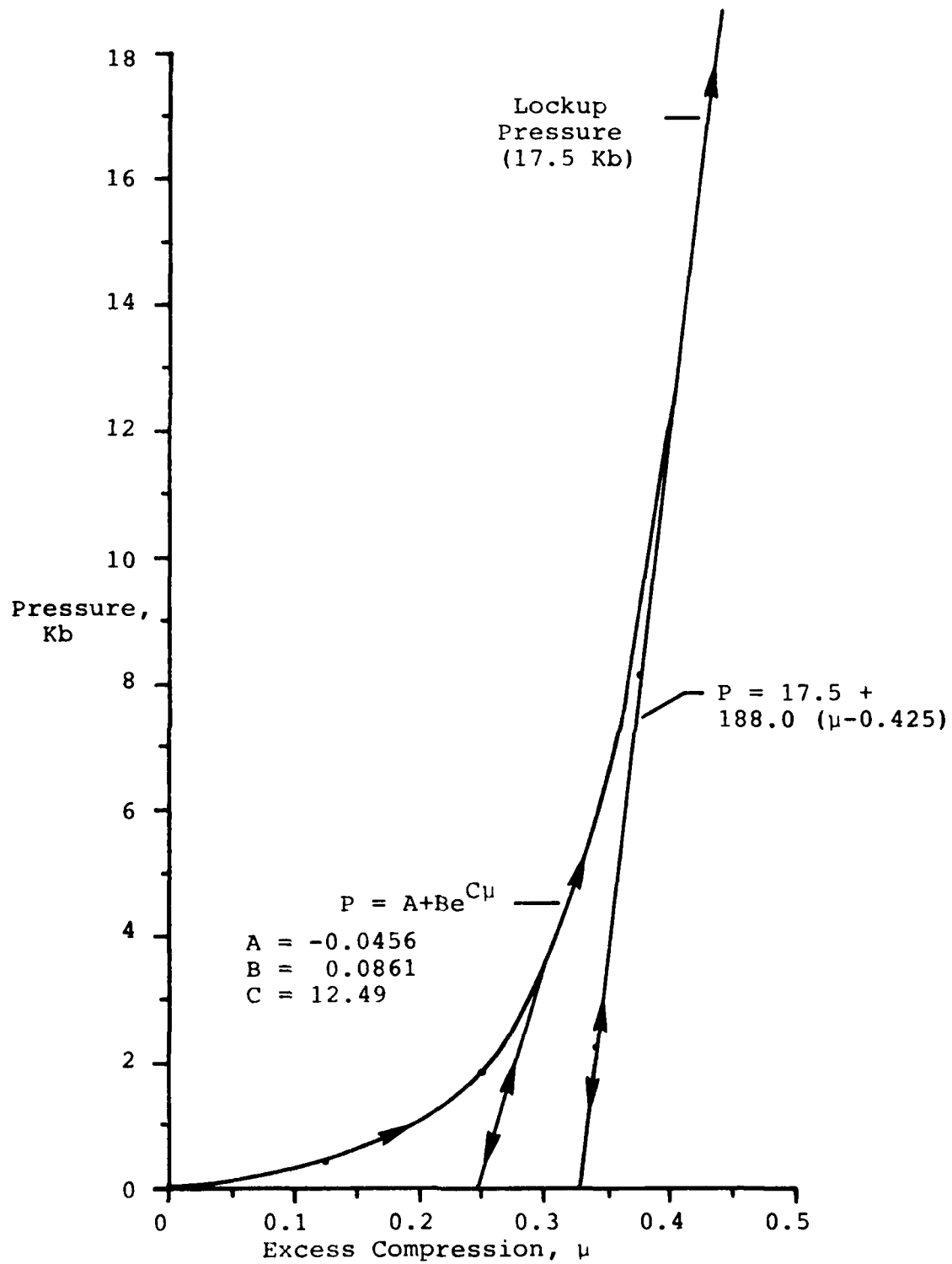Figure 3. Sand Hydrostat to 18 Kilobars.

The figure shows a plot of Pressure, Kb (y-axis, 0 to 18) versus Excess Compression, μ (x-axis, 0 to 0.5).

Lockup
Pressure
(17.5 Kb)

$P = 17.5 + 188.0 (\mu - 0.425)$

$P = A + Be^{C\mu}$

A = -0.0456
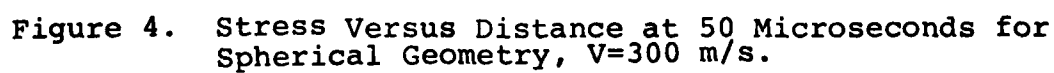B = 0.0861
C = 12.49

SECTION III

HYDROCODE CALCULATIONS

Two types of calculations were undertaken in this effort: loading calcu-
lations on concrete slabs, and penetration calculations. The loading calcula-
tions were undertaken to investigate attenuation of stress waves in concrete
in cylindrical and spherical geometries, and reflections from free (air-
backed) and sand-backed surfaces. Loading was induced by driving a concrete
surface at a given velocity level. These calculations were performed in the
two-dimensional Lagrangian hydrocode, TOODY (Reference 6).

Figures 4 and 5 present stress (in dynes/cm²) vs distance (in cm) in a
spherically diverging wave induced in concrete. The label TXX refers to total
stress and X refers to distance. The numbers on the curve refer to grid index
values in the calculation. The figures show stress at 50 and 90 microseconds.
The stress is induced by driving the inner spherical surface at $3x10^4$ cm/s
(300 m/s). The figures clearly show the lead advance of the elastic precursor
followed by a sharp rise to the peak stress induced by the 300 m/s velocity.
This peak stress level is seen to attenuate with distance into the concrete
(with divergence of the wave). For example, at 50 μs the peak stress at the
shock front is approximately $5x10^9$ dynes/cm² (5 Kb). At 90 μs this peak has
decayed to approximately 3 Kb. Examination of data from this calculation
indicates that peak loading stress varies with radial distance (to within 10
percent) according to the equation:

$$\tau(R) = \left(\frac{R_o}{R}\right)^{0.8} \tau_o$$

where τ_o is the stress at radius R_o and $\tau(R)$ is the stress at radius R. The
calculation also indicates that the elastic precursor advances at a velocity
close to 5 km/s while advance of the peak stress is a more sedate 3.3 km/s.

Figures 6 through 9 provide calculational predictions for the same
loading in cylindrical geometry at 50, 100, 150 and 200 μs. The peak stress
in this case is fit (again to within 10 percent) by:

11

Figure 4.   Stress Versus Distance at 50 Microseconds for
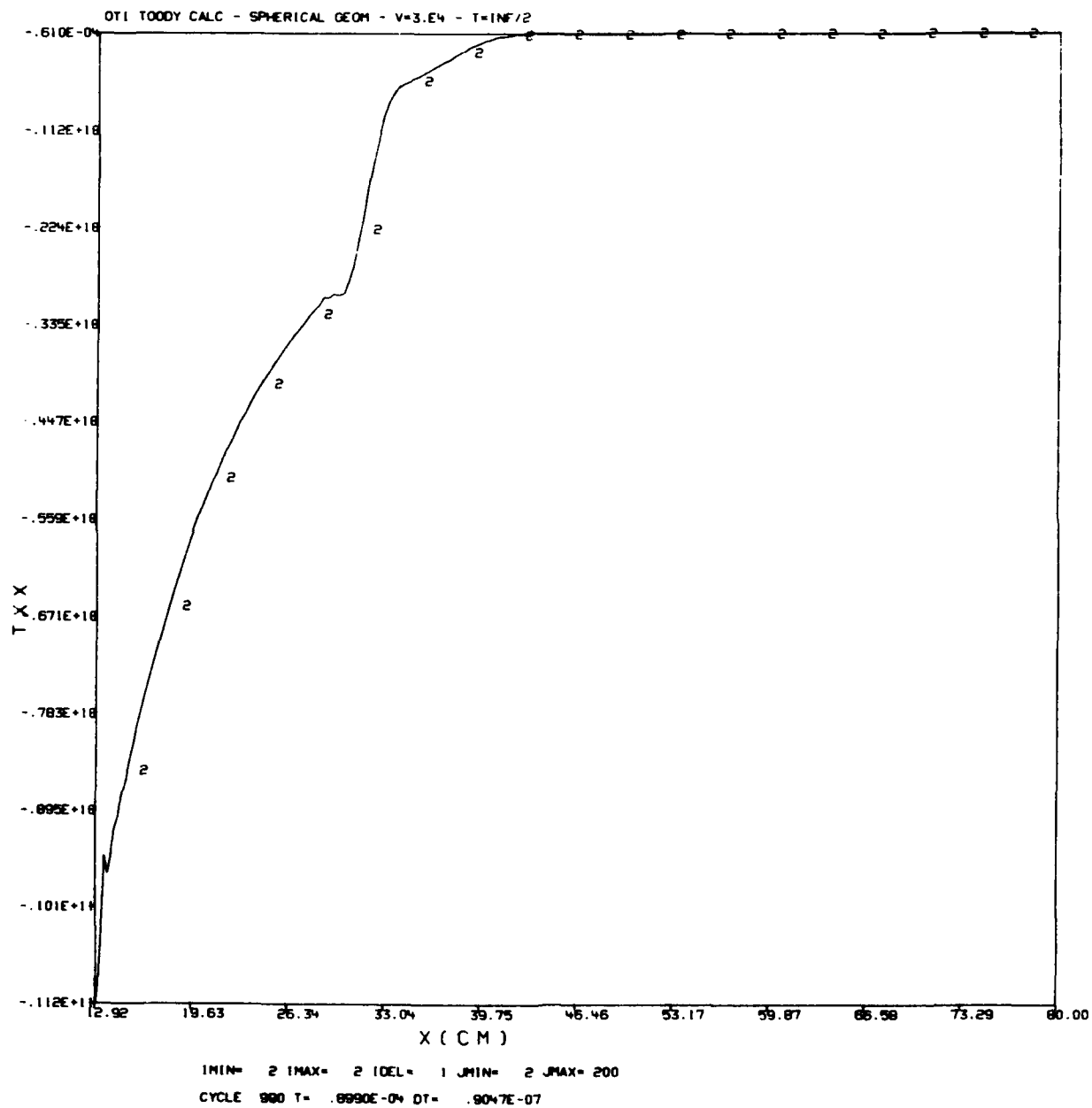   Spherical Geometry, V=300 m/s.

12

Figure 5.   Stress Versus Distance at 90 Microseconds
for Spherical Geometry, V=300 m/s

13

Figure 6. Stress Versus Distance at 50 Microseconds for Cylindrical Geometry, V=300 m/s.

14

Figure 7. Stress Versus Distance at 100 Microseconds for Cylindrical Geometry, V=300 m/s

15
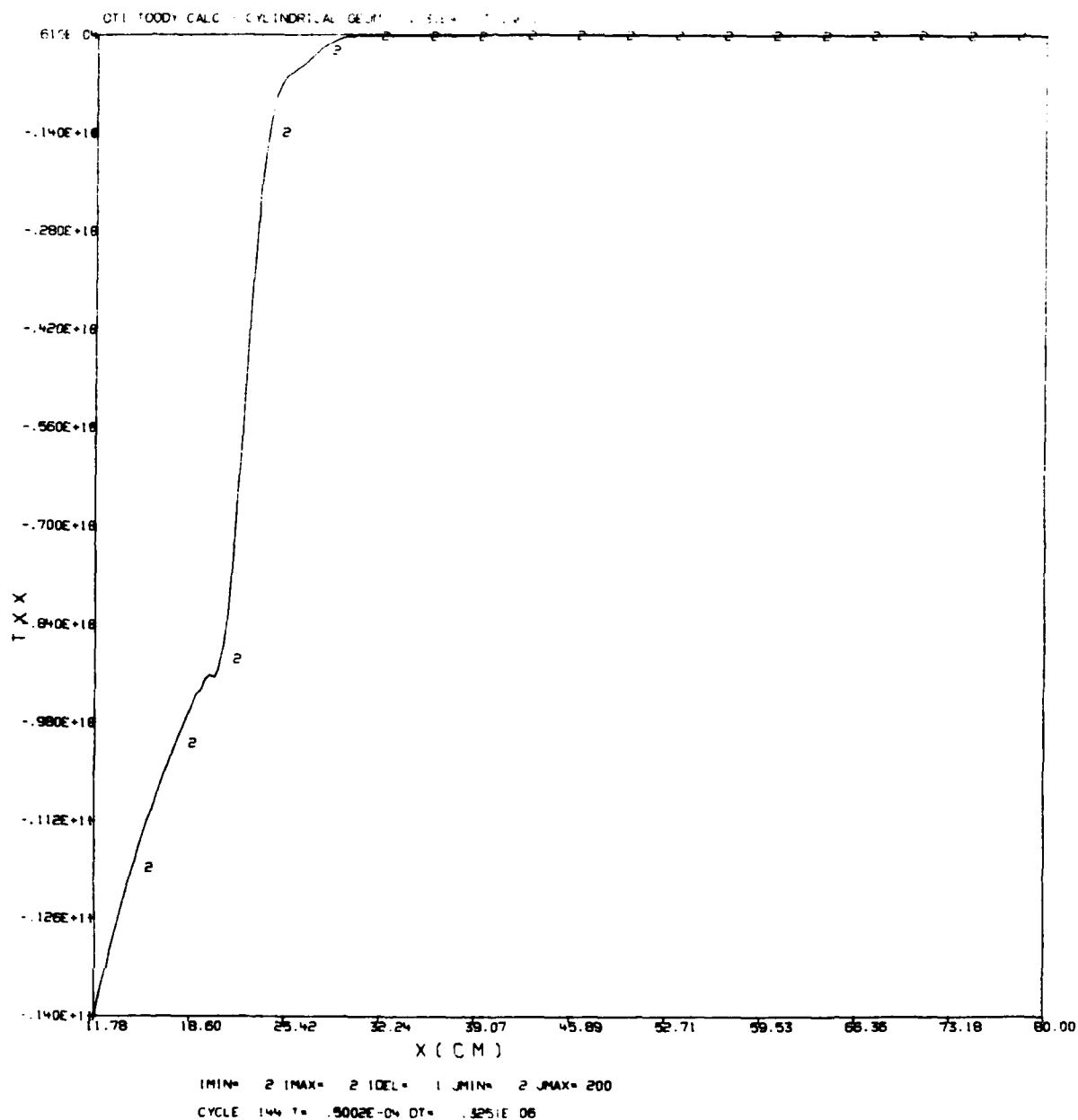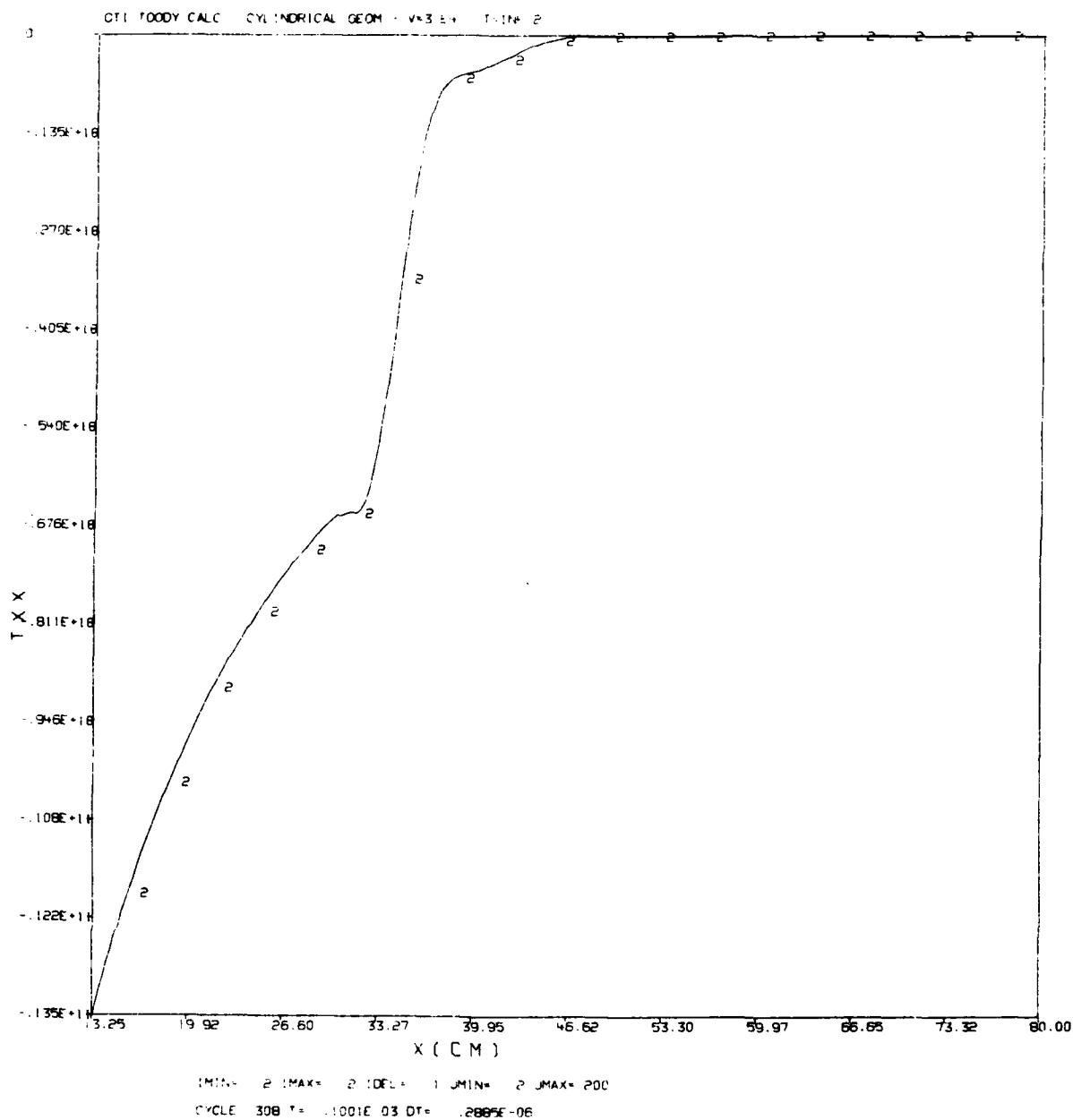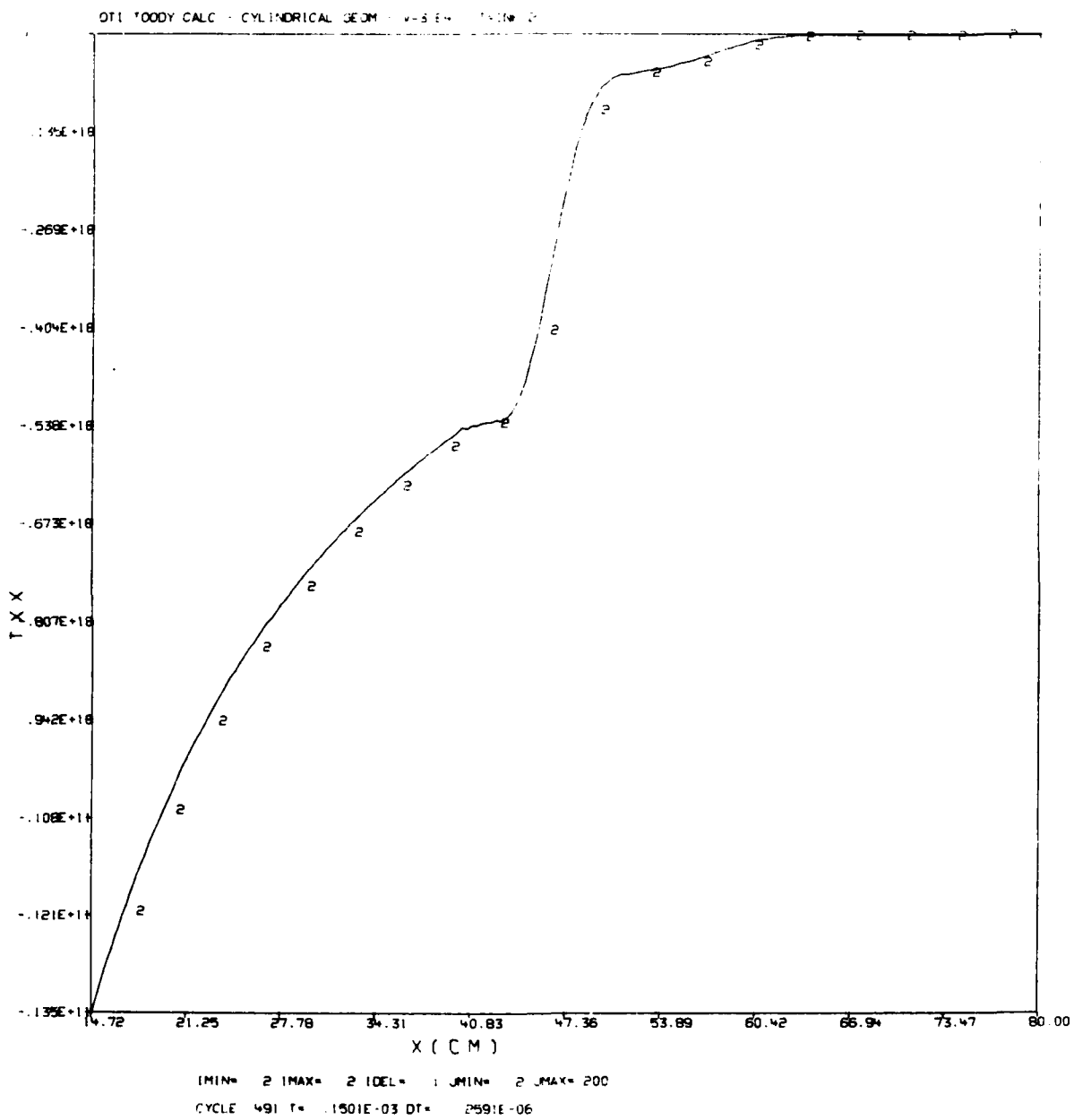
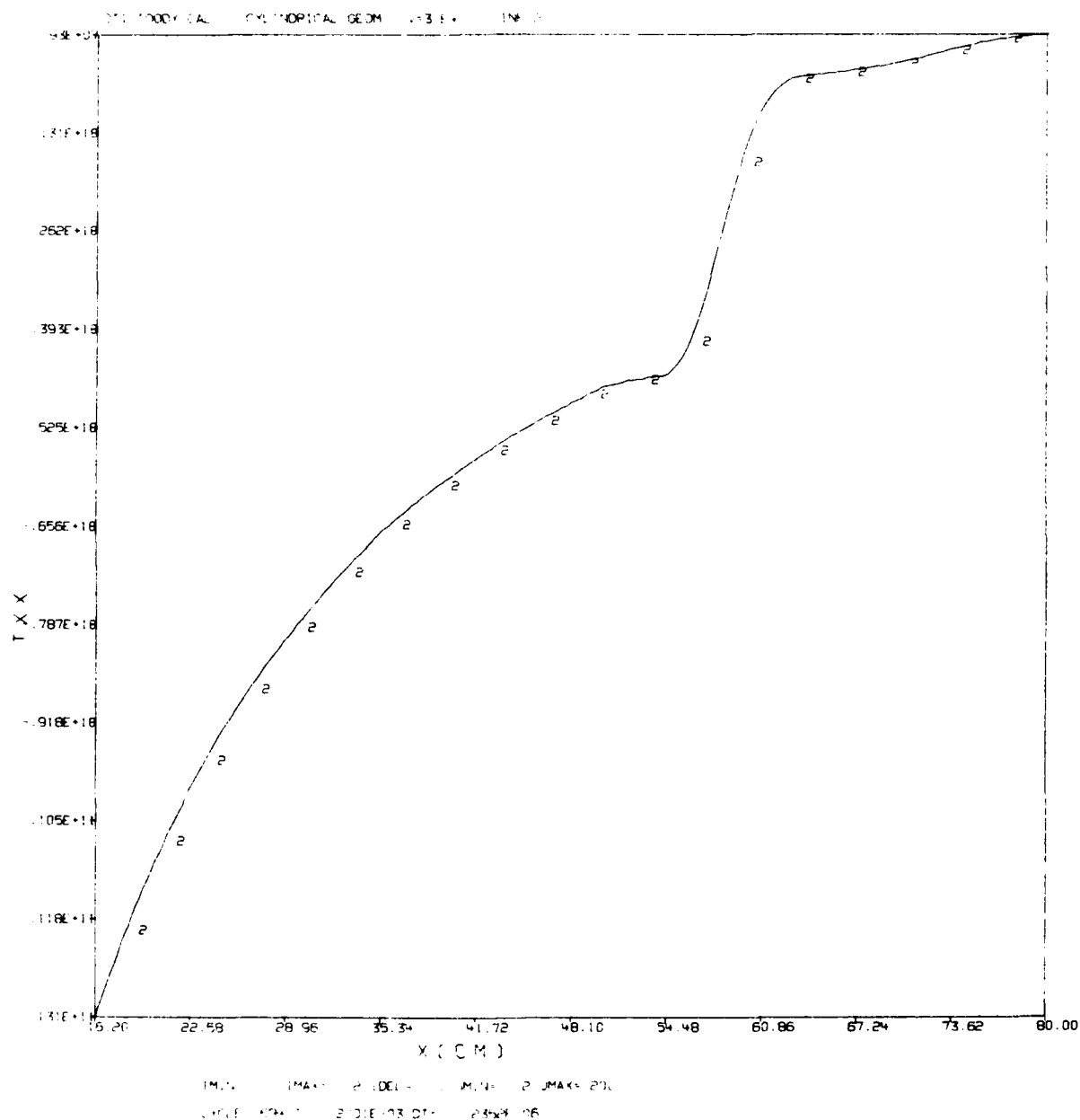Figure 8. Stress Versus Distance at 150 Microseconds for Cylindrical Geometry, V=300 m/s.

Figure 9.   Stress Versus Distance at 200 Microseconds for
            Cylindrical Geometry, V=300 m/s.

17

$$\tau(R) = \left(\frac{R_o}{R}\right)^{1.6} \tau_o$$

Again, the elastic precursor is seen to separate and outrun the peak stress wave.

The calculations discussed above were performed in semi-infinite concrete. Were the concrete of finite extent, of course, the loading within the concrete would be considerably different due to reflections from the interface between the concrete and the next medium. As an example of this effect, consider the case for a concrete slab 10-cm thick, backed by semi-infinite sand. Consider also that the entire free surface (top) of the slab is given a sustained velocity of 300 m/s. This is, of course, plane geometry and there should be no stress attenuation due to divergence. Figures 10 through 15 show how stress will vary with distance in the concrete and sand at 50, 100, 150, 200, 250 and 400 µs. In Figure 10, it is seen that, at 50 µs, the initial stress wave of approximately 17 Kb has been reduced to 9 Kb at the sand/concrete interface by a relief wave propagating from the interface back into the concrete. By 100 µs, Figure 11, the relief wave has reached the moving concrete surface and reduced the stress at that point to 6 Kb. Figures 12, 13 and 14 show the stress settling down to a value slightly over 6 Kb as wave fronts settle down and the concrete/sand combination begins moving at the same velocity. The stress is almost a constant 6.5 Kb at 400 µs (Figure 15) across the concrete and sand. The only disturbance exists at the initial wave front which is now deeply in the sand.

Figures 16 through 19 are stress vs time plots for stations just inside the concrete (Figure 16), midway into the 10-cm concrete slab (Figure 17), in the concrete at the sand interface (Figure 18) and in the sand just across the interface (Figure 19). The plots labelled 'RAD STRESS – KB' present stress vs time for the stress component in the direction of slab motion. The plots labelled 'AX STRESS – KB' present the same information for the other component of stress (i.e., the one normal to the direction of motion). Examination of Figure 16 shows that a peak stress of 17.2 Kb is reached just inside the concrete's surface in approximately 10 µs. The stress remains at this level until 50 µs at which time the relief wave from the concrete/sand interface

18

Figure 10. Stress Versus Distance at 50 Microseconds, Plane Geometry, 10-cm Concrete/Sand, V=300 m/s.

Figure 11. Stress Versus Distance at 100 Microseconds, Plane
Geometry, 10-cm Concrete/Sand, V=300 m/s.

20

Figure 12. Stress Versus Distance at 150 Microseconds, Plane Geometry, 10-cm Concrete/Sand, V=300 m/s.

21

Figure 13. Stress Versus Distance at 200 Microseconds, Plane
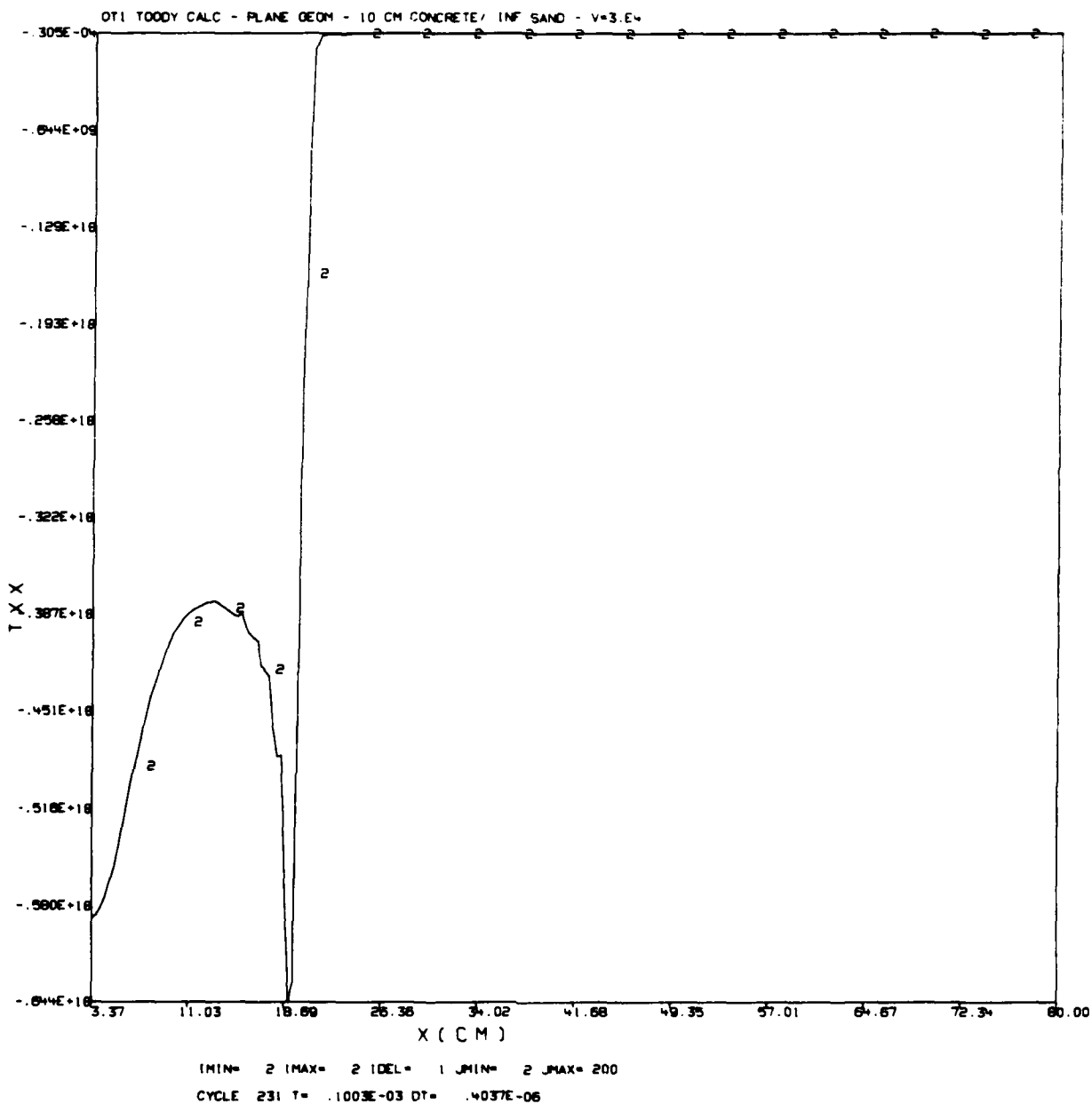Geometry, 10-cm Concrete/Sand, V=300 m/s.
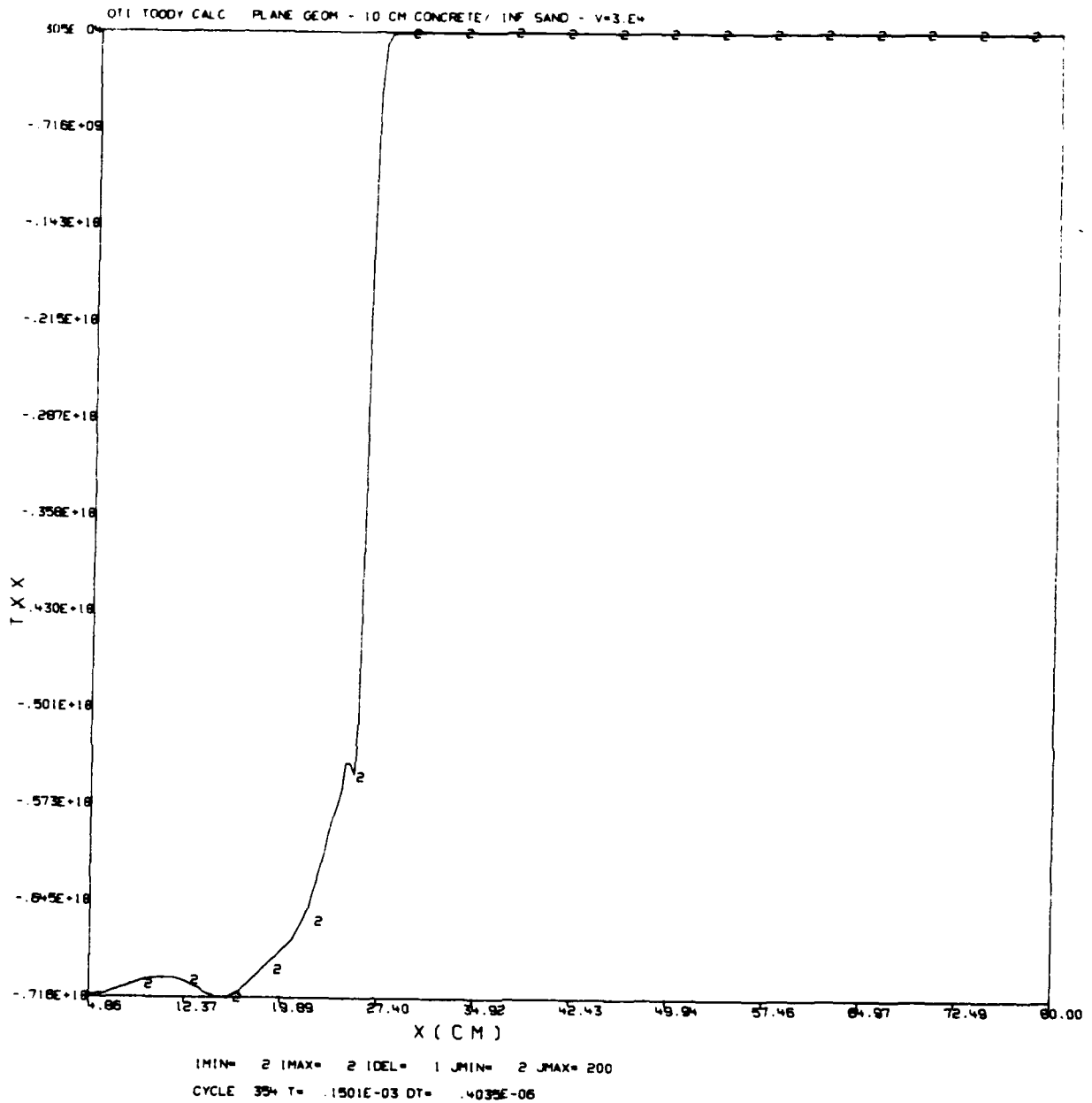
22
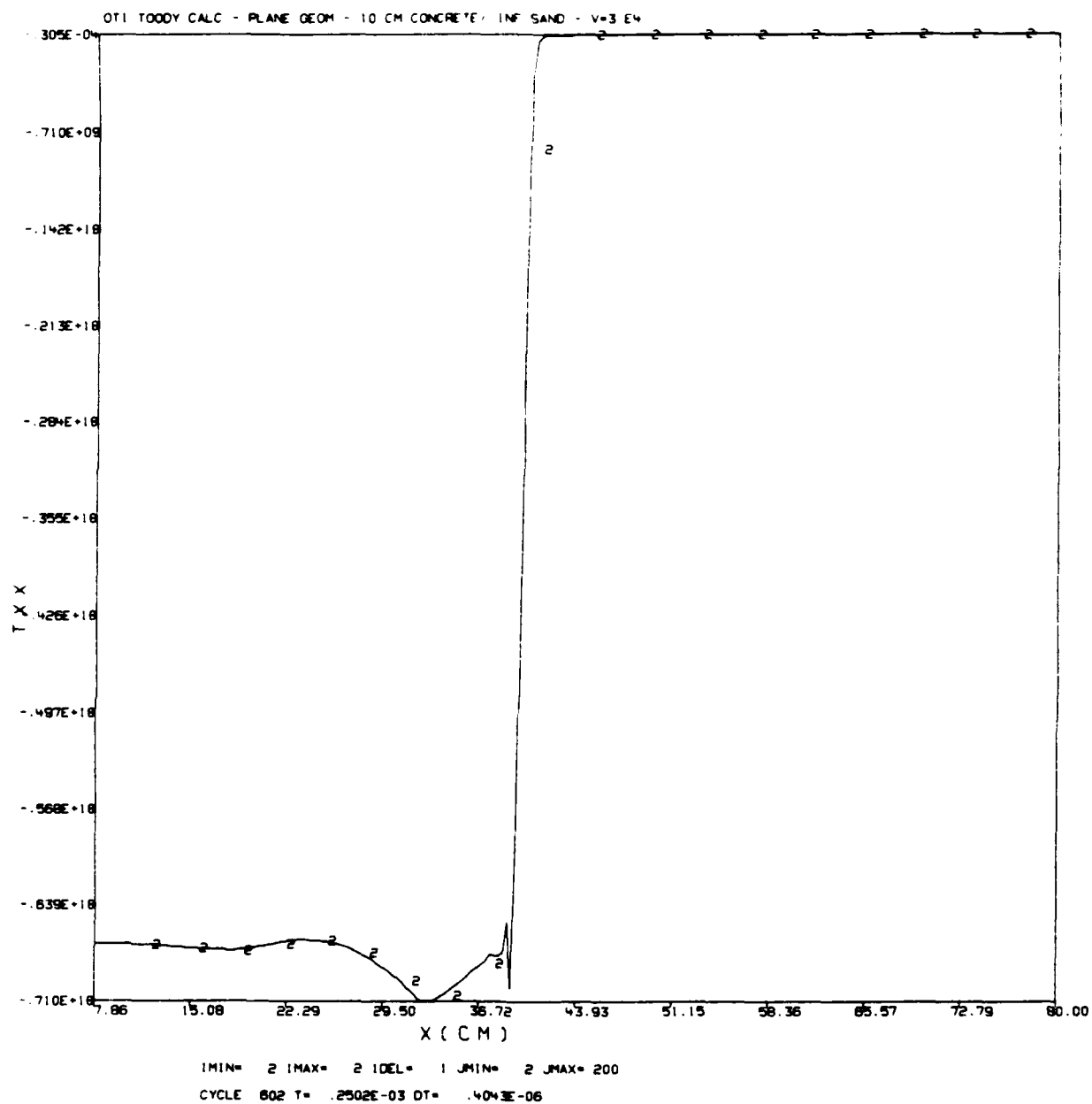
Figure 14.   Stress Versus Distance at 250 Microseconds, Plane
             Geometry, 10-cm Concrete/Sand, V=300 m/s.

Figure 15. Stress Versus Distance at 400 Microseconds, Plane Geometry, 10-cm Concrete/Sand, V=300 m/s.
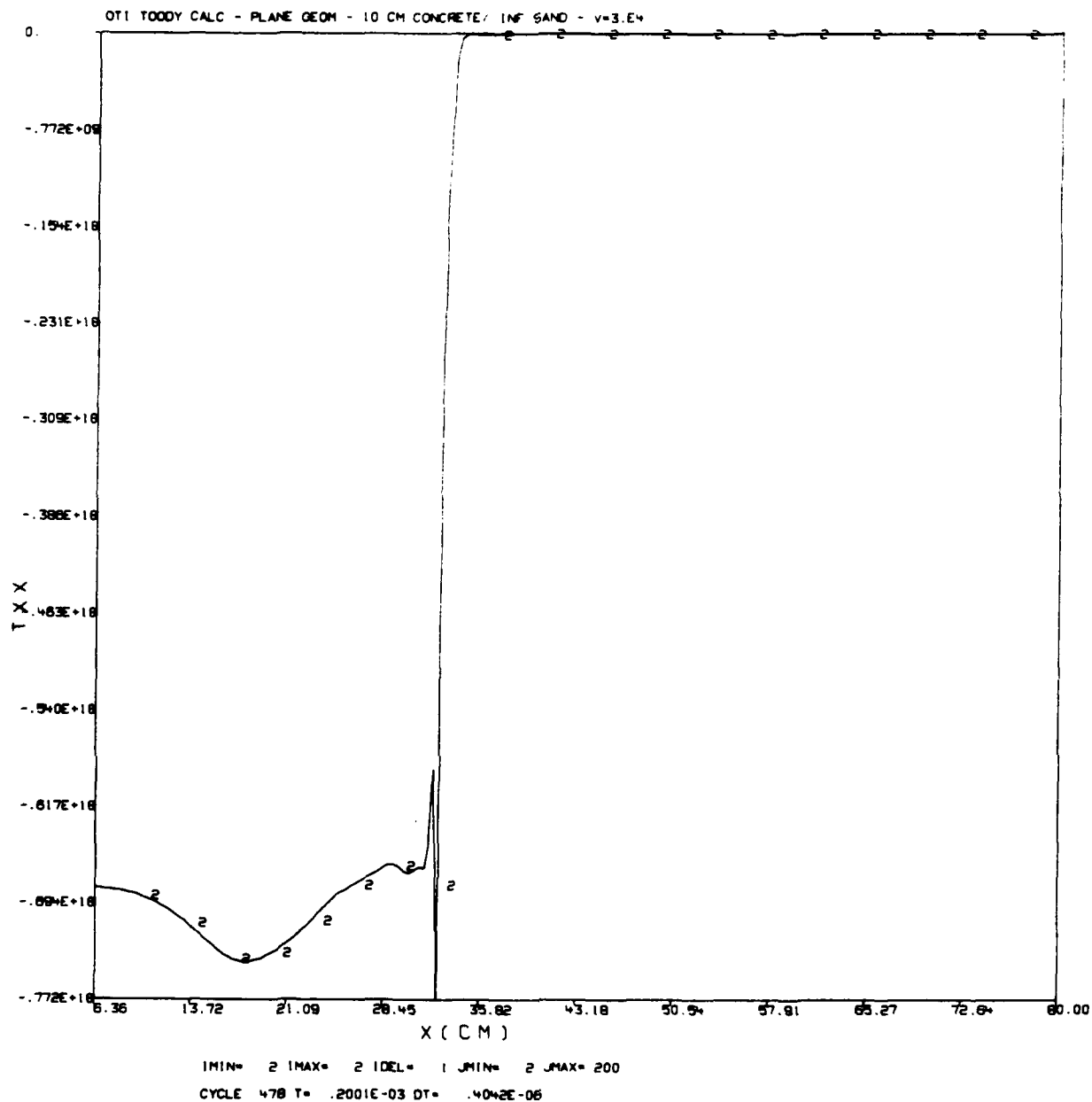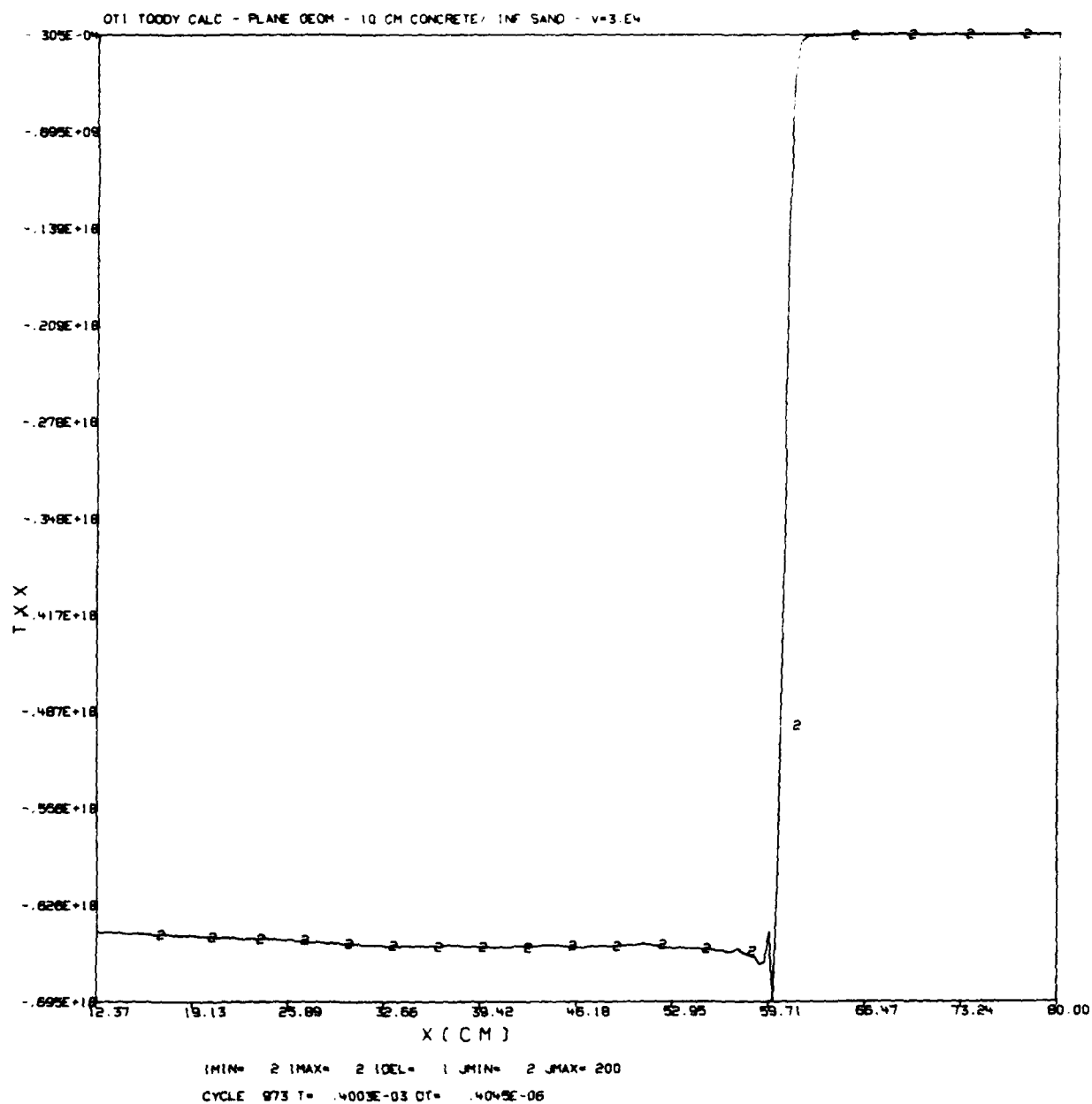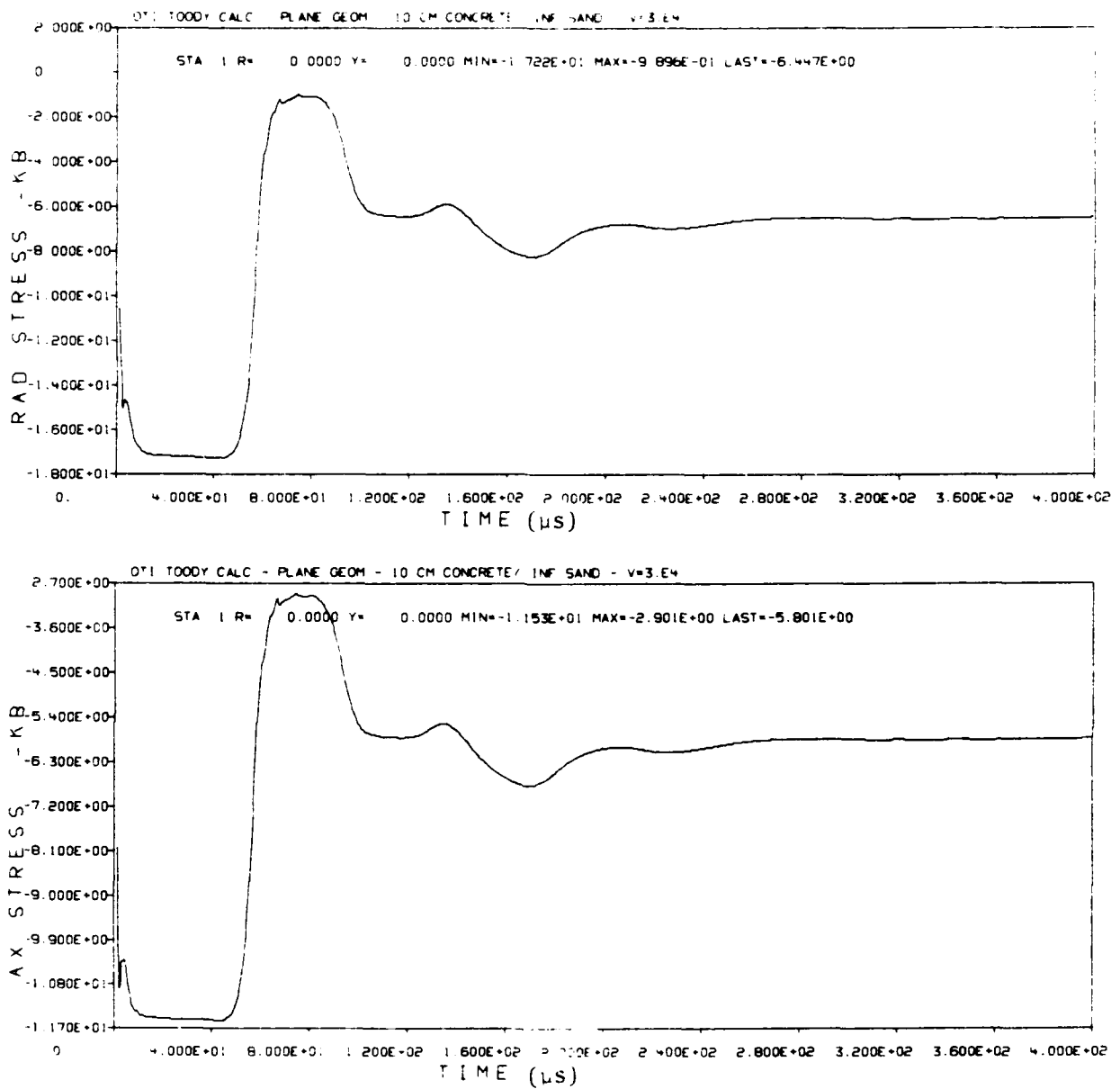
24

Figure 16. Stress Versus Time at A Point Near the Concrete Surface.
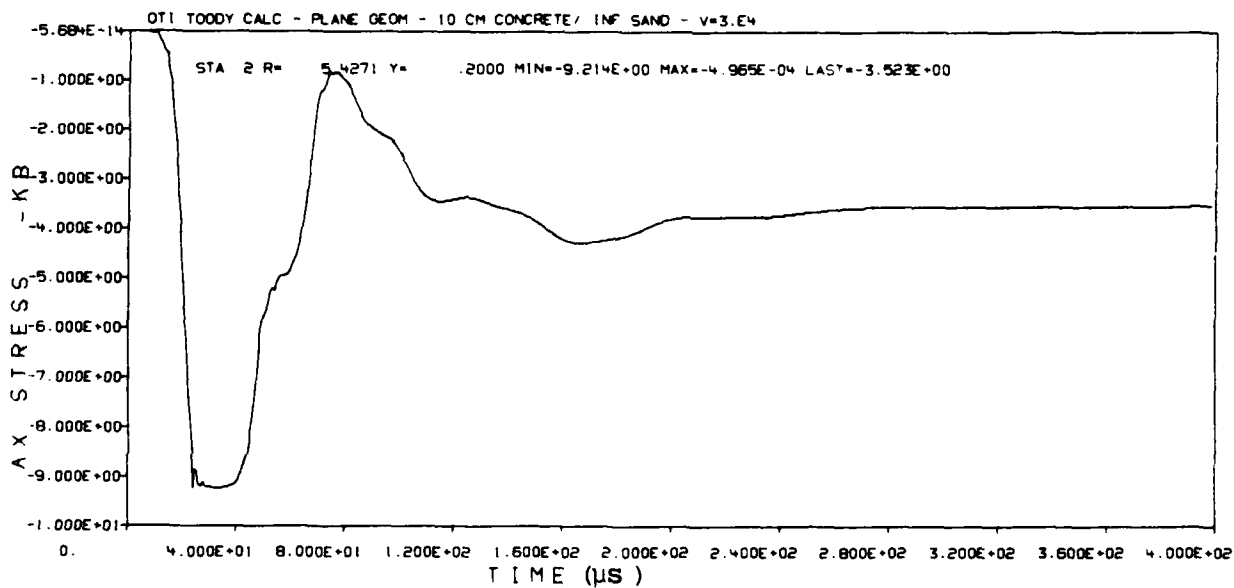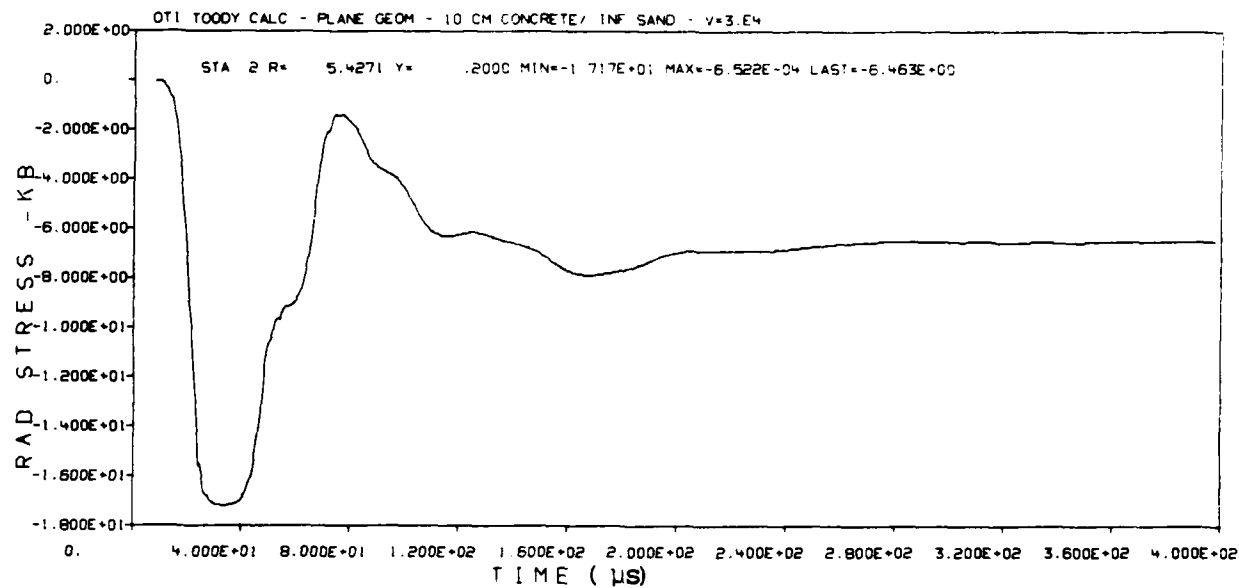
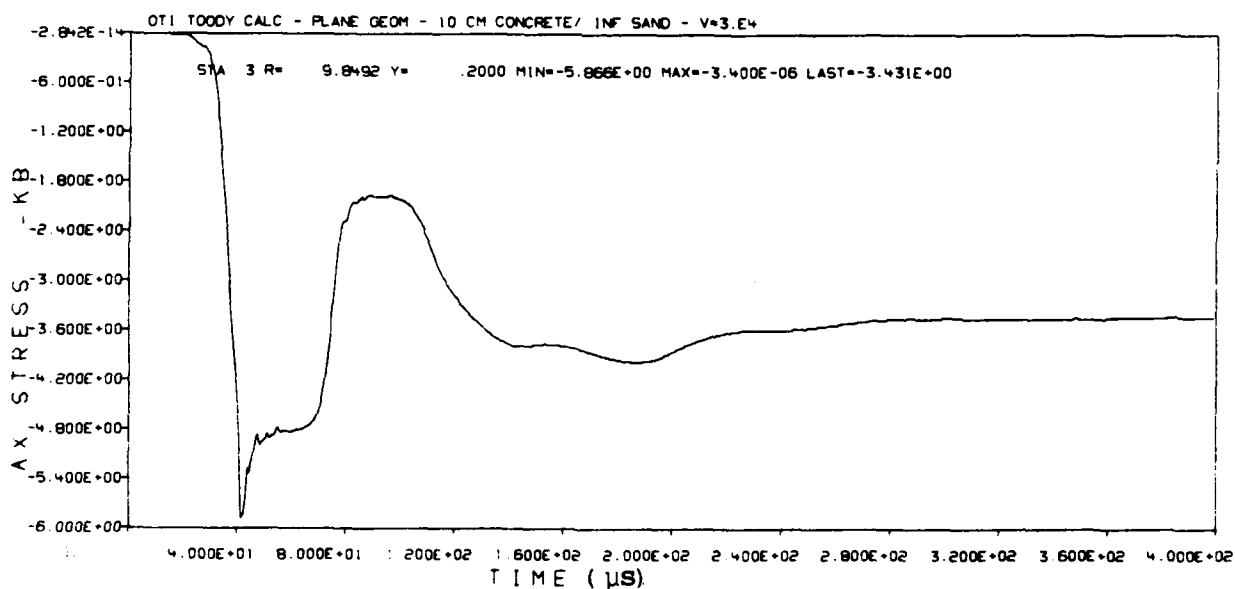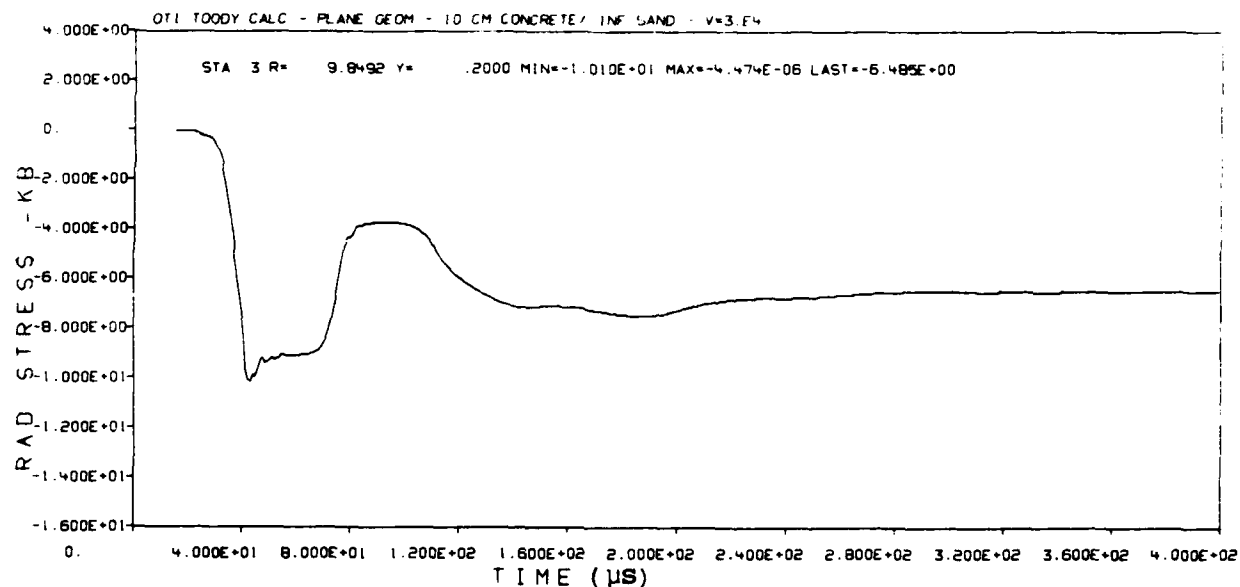Figure 17. Stress Versus Time at A Point Midway in the Concrete Slab.

26

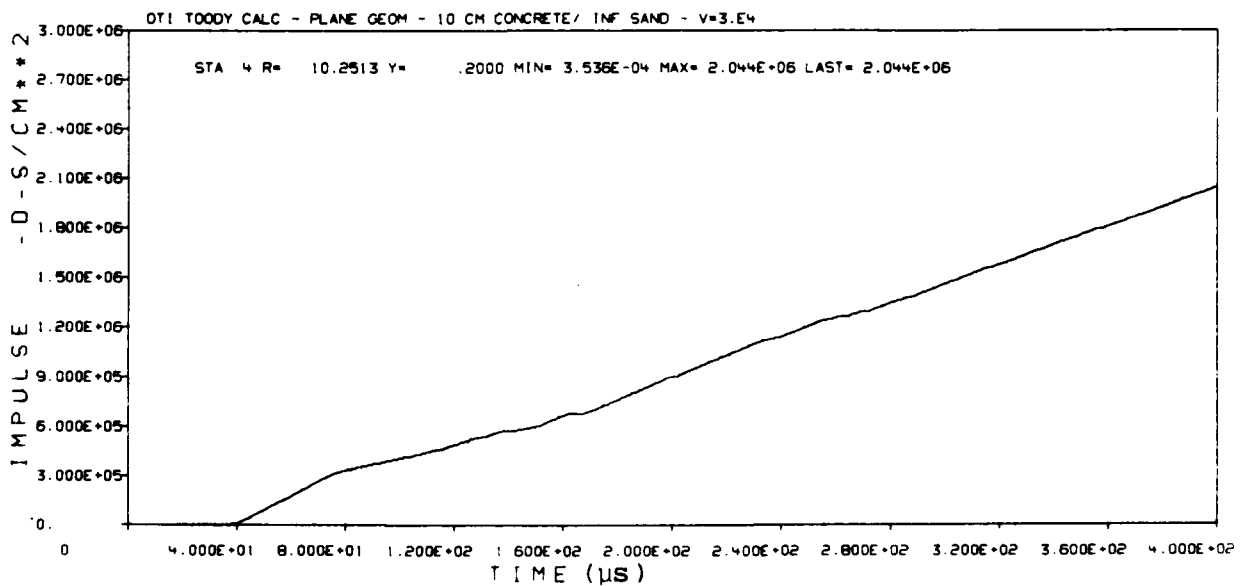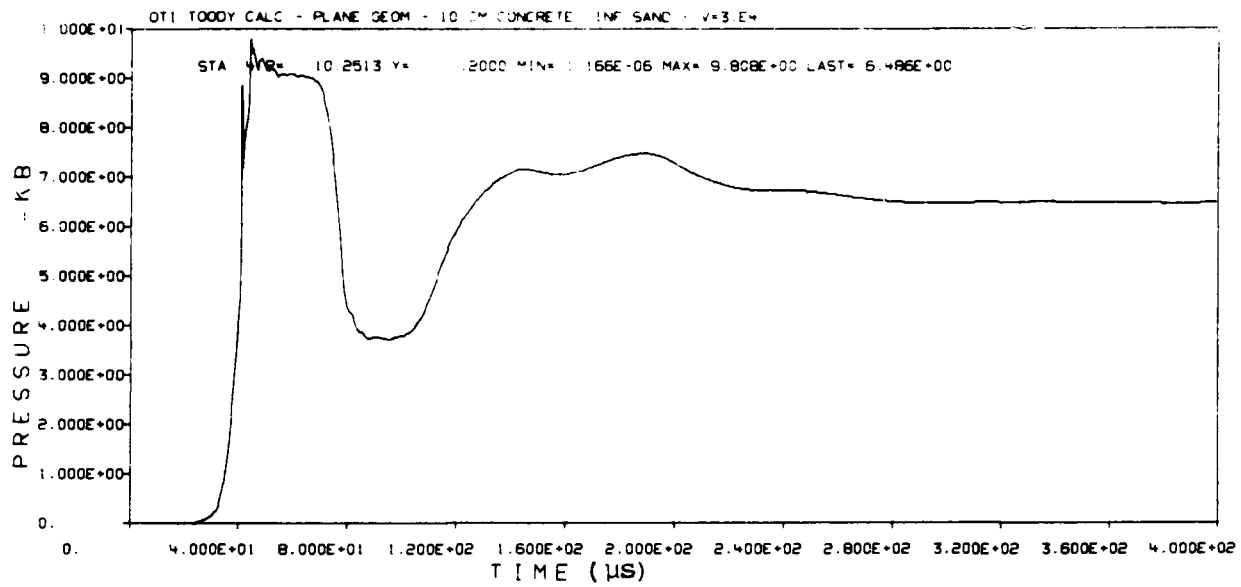Figure 18. Stress Versus Time at A Point in the Concrete at the Sand Interface.

Figure 19. Stress Versus Time at A Point in the Sand at the Concrete Interface.

28

arrives. Stress immediately drops to a nearly zero value and then slowly builds up to a steady value of 6.5 Kb. Figure 17 is very similar, with the exception that the initial 17.2 Kb peak is more short-lived due to the shorter distance to the interface. Figure 18 illustrates that concrete at the interface is not allowed to reach the 17 Kb level. It reaches a peak of approximately 10 Kb because of the relief at that interface. Figure 19 shows the same data in the sand at the interface. There is a reversal of sign because the sand has no strength and only pressure can be plotted. It can be stated that an interface with sand will reduce stress loading to a small fraction (1/3 in the specific case investigated) of the original loads.

The stress field providing loading on a projectile is very complex, as seen in Reference 1, and cannot be equated to that resulting from spherical or cylindrical divergence. So it is not possible to apply the results of the previous calculations directly to the case of an actual penetration. However, much of the phenomenology will be similar--i.e., the stress wave will attenuate as it propagates into the concrete and return from the interface as an unloading wave. This unloading wave will reduce the stress seen by the projectile. Loading on the projectile can, therefore, be expected to be a strong function of the concrete's thickness and the amplitude of the initial stress wave (i.e., the velocity of the projectile). In addition, it can be expected that some aspects of the loading will be a function also of the projectile's diameter.

Penetration calculations were undertaken, primarily with blunt projectiles at velocities of 100, 200, 300 and 500 m/s. The projectiles were 1 or 2 cm in radius and the target thicknesses varied from 2.5 to 10 cm. The actual values of projectile diameter and target thickness employed in the calculations are not important since the loading data will scale with these dimensions. Most concrete slabs were backed with dry sand. A few runs were made with air backing. Runs with conically-nosed projectiles were made at 300 and 500 m/s.

Figures 20 and 21 show density contours from a typical blunt nose calculation. The calculations were performed using the Eulerian HULL code (REF 7). Figure 20 shows the initial geometry for a 1-cm radius projectile impacting a
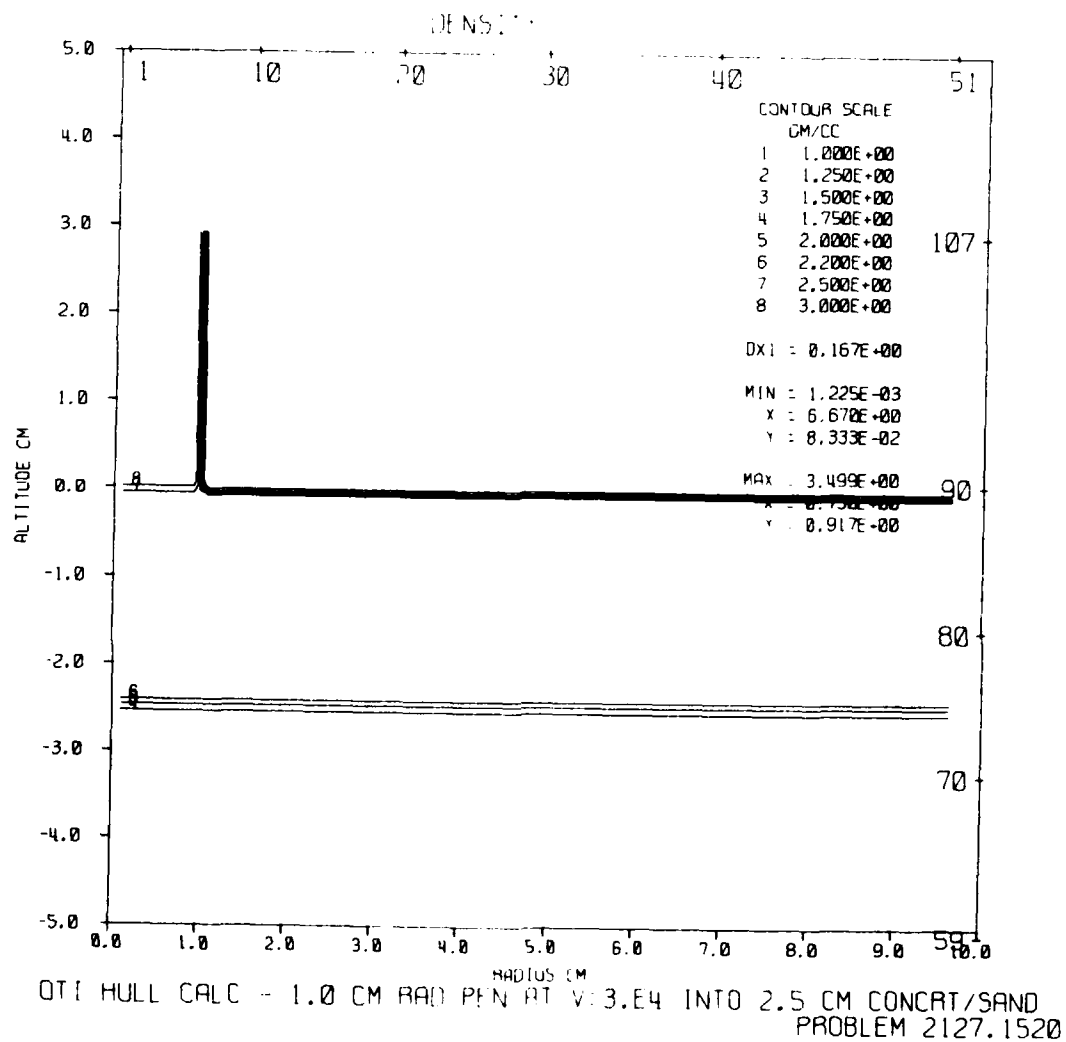
29

Figure 20. Initial Conditions for 1-cm Radius Blunt
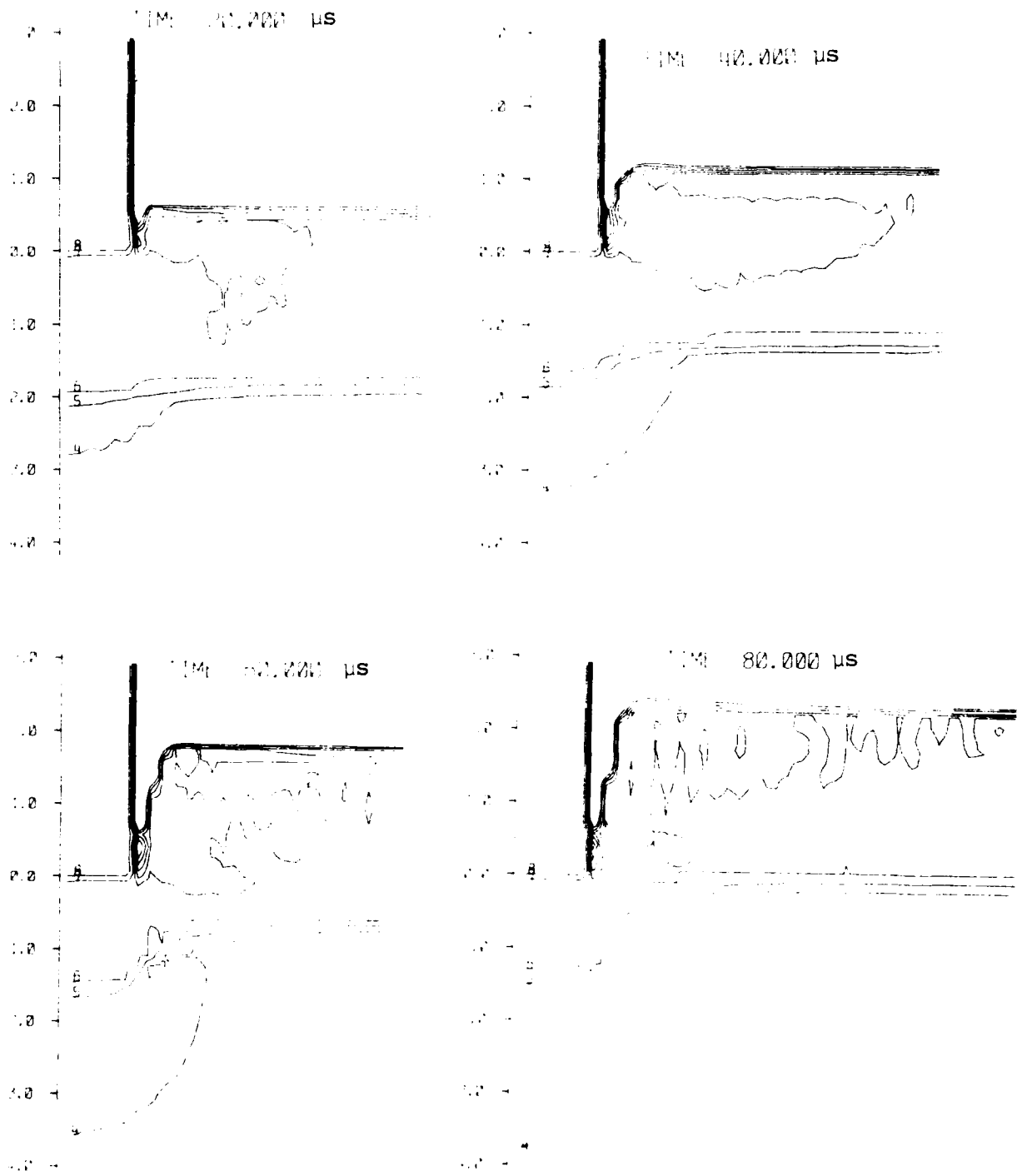Penetrator Impacting 2.5 cm Sand-backed
Concrete.

Figure 21. Density Contours of 1-cm Radius Blunt Penetrator Impacting 2.5 cm Sand-Backed Concrete.

31

sand-backed, 2.5-cm thick concrete slab. The vertical axis is an axis of rotational symmetry so only one-half of the problem need be simulated. Figure 21 shows density profiles of the penetration event at 20, 40, 60 and 80 μs. By this last time, the projectile is even with the bottom of the concrete slab and is pushing a large section of concrete ahead of it into the sand. The calculation was actually run with the projectile fixed in space and the concrete/sand driven into it at 300 m/s. Stresses were collected at each time step for the six zones across the front of the projectile. These stresses were multiplied by the appropriate zone areas to obtain total force on the projectile. This force was then divided by the projectile's total nose area to obtain the loading stress. The projectile was not allowed to decelerate for these calculations so that stress loading at a given velocity level could be developed.

Stress vs time curves for these blunt projectiles are seen in Figures 22 through 25. Each figure shows loading curves for several concrete thicknesses and a given projectile velocity. On each figure, the stress vs time curve for semi-infinite concrete is also shown.

Figure 22 presents blunt 1-cm radius projectiles impacting sand-backed concrete of 5-cm, 10-cm and semi-infinite thickness. The loading curve for the 10-cm and semi-infinite concrete are essentially identical. The curve for the 5-cm concrete is also identical with the exception of a 40 μs loss of pressure due to the return of the peak stress from the sand interface. For 10 cm and beyond, this peak stress is too attenuated to be seen at the projectile.

Figure 23 shows loading from the same three concrete thicknesses for a projectile travelling at 200 m/s. With the exception again of a short-lived drop in stress for the 5-cm concrete, there is essentially no difference in loading on the projectile.

At 300 m/s, Figure 24, significant loading differences begin to appear. The 5-cm thick concrete curve is an average of 4 Kb below the 10-cm and semi-infinite loading curves. A 2.5-cm thickness was also investigated for this velocity. The drop to a 2.5-cm thickness decreased loading by another
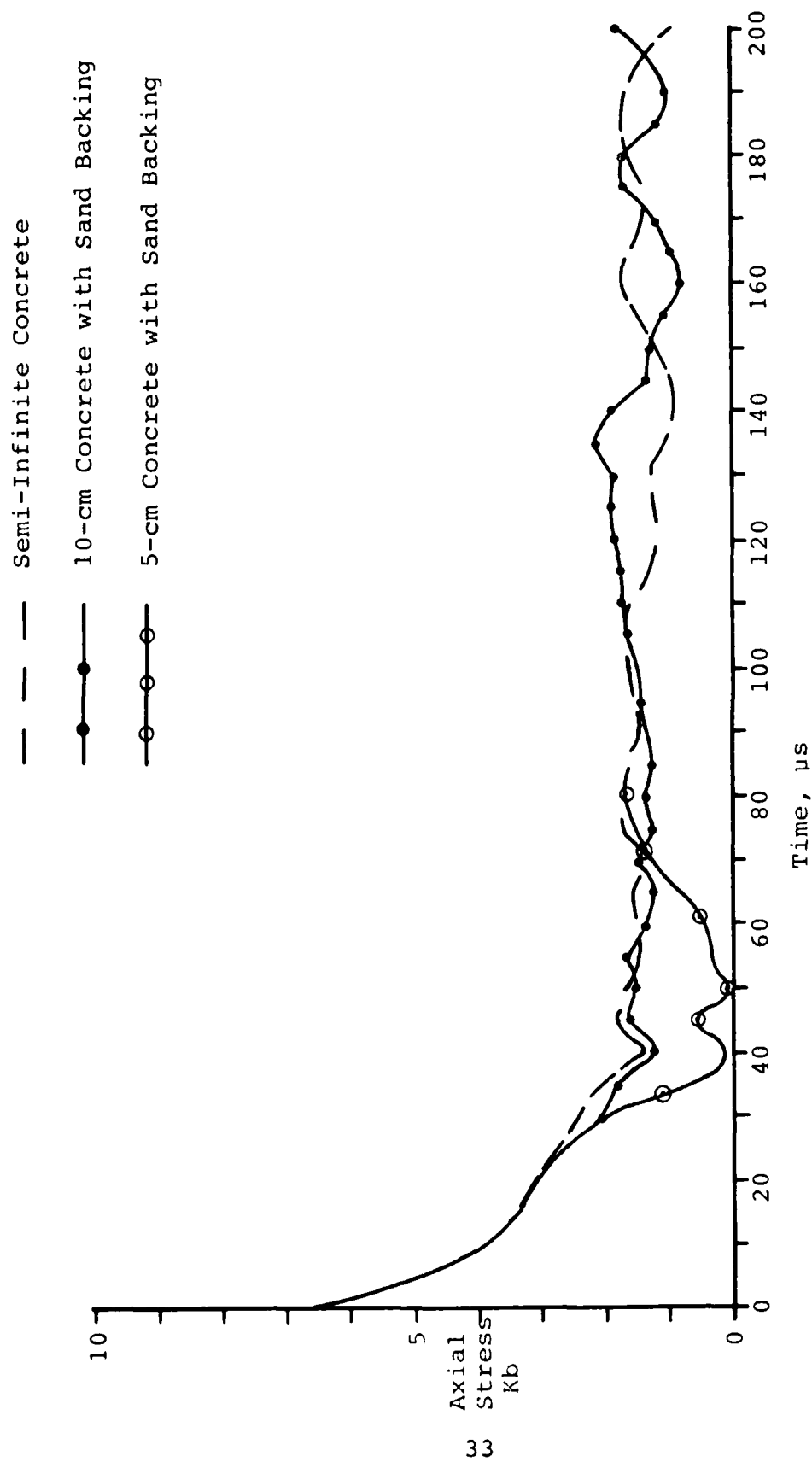
32

Figure 22. Blunt 1-cm Radius Projectiles at 100 m/s Impact Velocity.
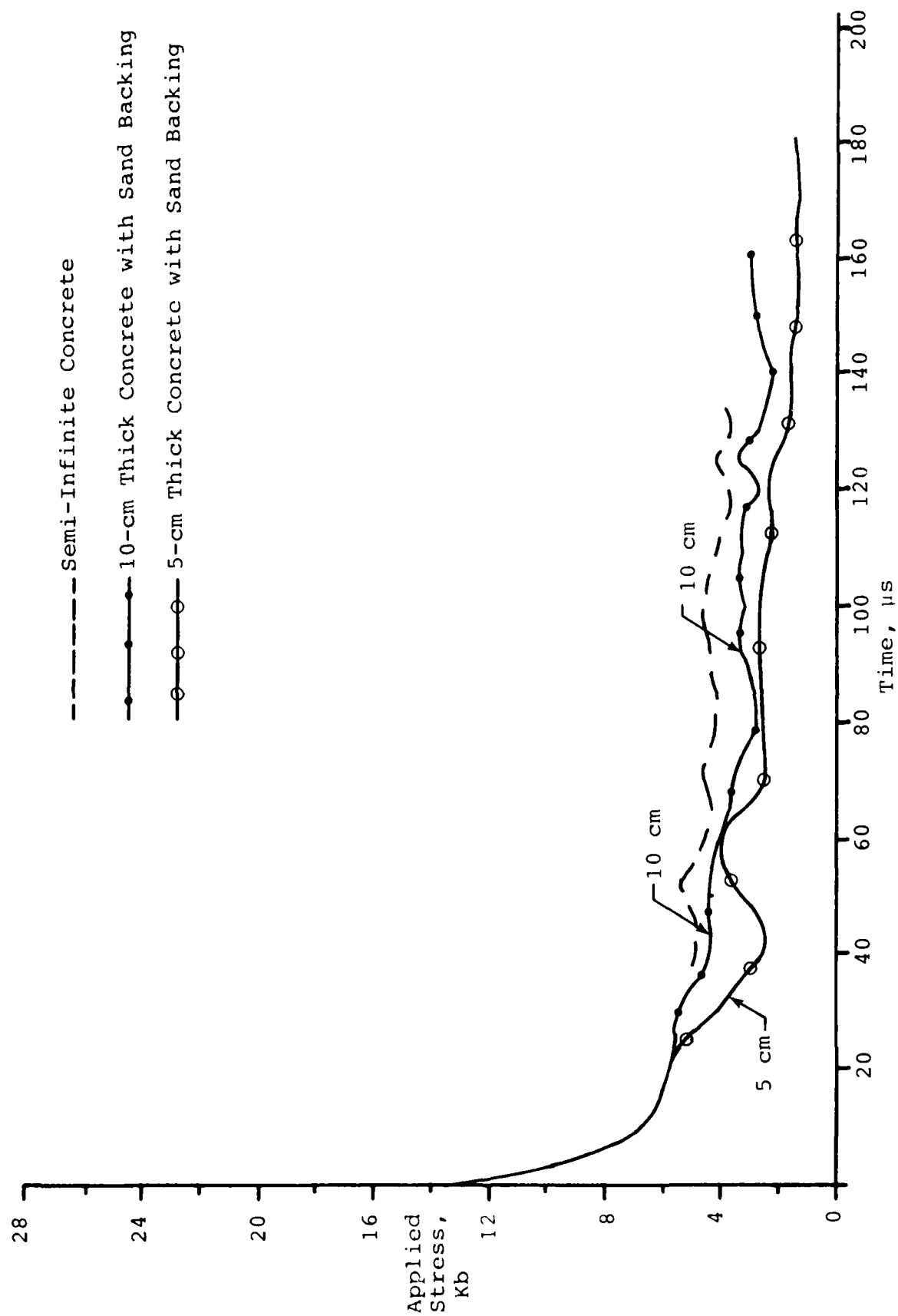
33

Figure 23. Blunt 1-cm Radius Projectiles at 200 m/s Impact Velocity.
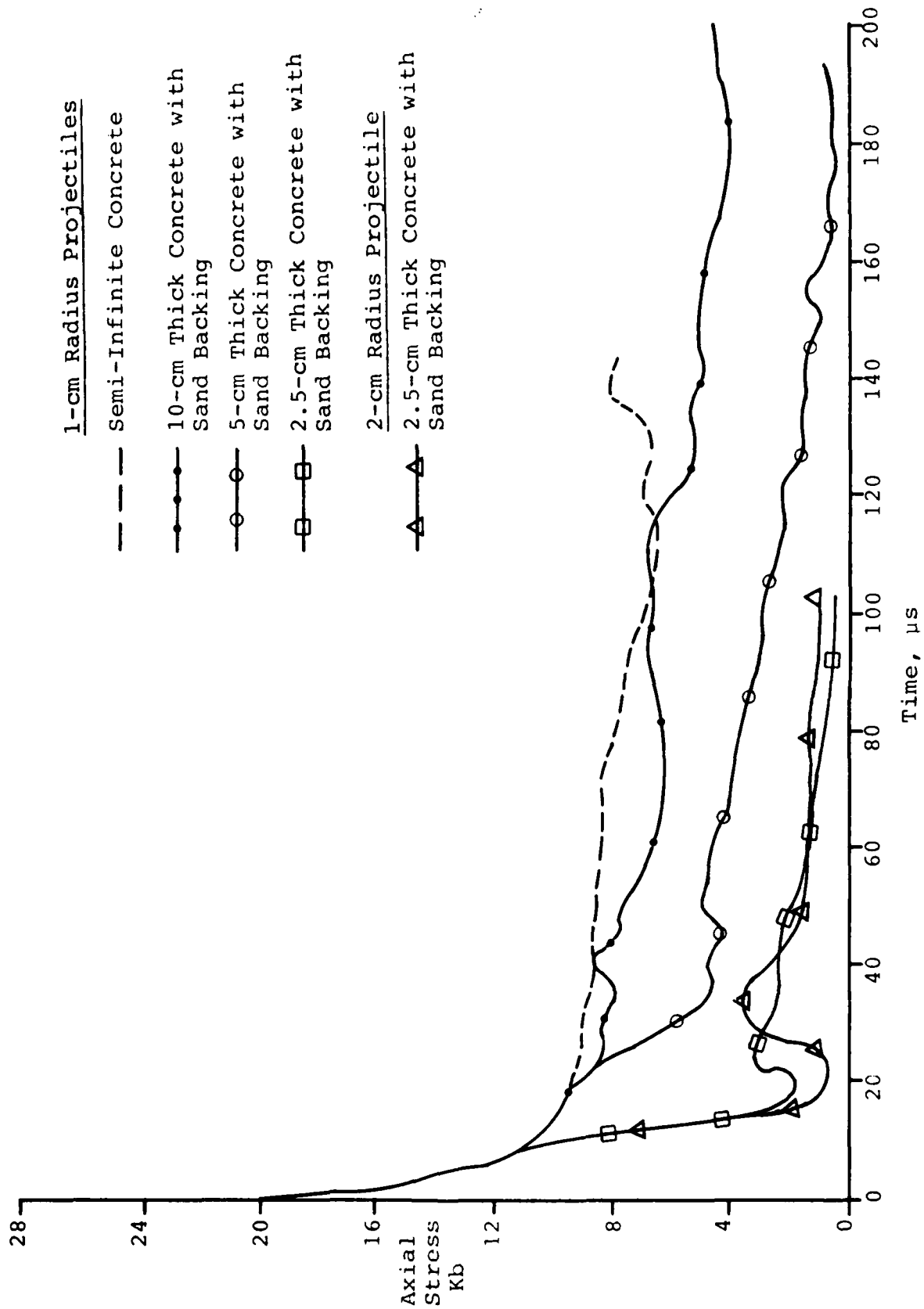
34

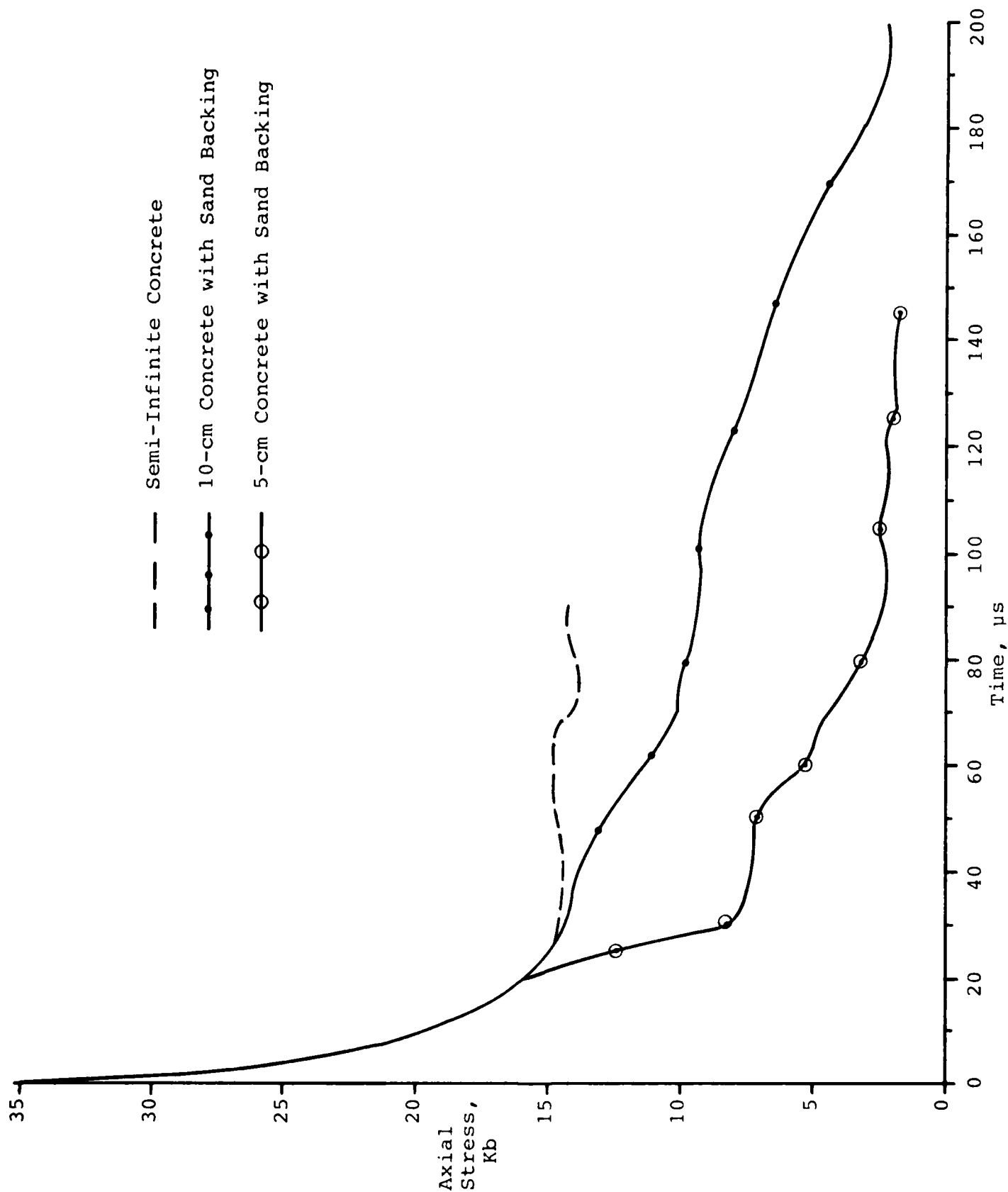Figure 24. Loading for Projectiles at 300 m/s Impact Velocity.

35

Figure 25.   Blunt 1-cm Radius Projectiles at 500 m/s Impact
             Velocity.

36

approximately 4 Kb. Also shown on this figure is the result of a 2-cm radius projectile impacting 2.5-cm thick concrete.

Figure 25 presents calculations for blunt projectiles impacting sand-backed concrete at 500 m/s. Stress drops due to unloading are seen to be very significant at this velocity level.

The fact that the total stress wave, including unloading, is a function of T/D (the concrete's thickness divided by the projectile's diameter) is seen in Figure 26. The two curves in this figure show projectiles at 300 m/s into sand-backed concrete. In one case, the projectile radius is 1 cm and concrete thickness is 5 cm. In the other curve, projectile radius is 2 cm and concrete thickness is 10 cm. The two curves, then, both have T/D values of 5. They would be virtually identical were time expressed in units of t/D. That is, the larger projectile reaches the same stress level, but at a later time. The ability to scale stress with time enables one to develop a model which will cover many situations with a relatively small number of calculations.

The difference between sand and air backing was investigated for projectiles at 300 m/s. The loading curves are seen in Figure 27 for 1-cm projectiles impacting 10-cm concrete, backed with air in one case and sand in another. There is some difference, but it is relatively small. Experimentally, little difference is seen between air and sand-backed concrete. It was decided, therefore, to assume that any model developed from sand-backed concrete calculations applies equally well to air-backed concrete.

Projectiles with conical noses were investigated at 300 and 500 m/s. Cone half angles were varied from 30 to 60 degrees. Each projectile was 1 cm in radius. Figure 28 presents loading on conically-nosed projectiles impacting sand-backed 5-cm thick concrete slabs at 300 m/s. As seen in the figure, there is little difference in axial stress on these projectiles after the entire cone has entered the concrete. The stress level lies along or slightly above the level for a blunt penetrator under the same impact conditions. This seemingly unusual circumstance occurs because the incident stress from a blunt projectile is higher and of longer duration than that from a cone resulting in a somewhat larger unloading wave. The stress in the figure is computed by

37
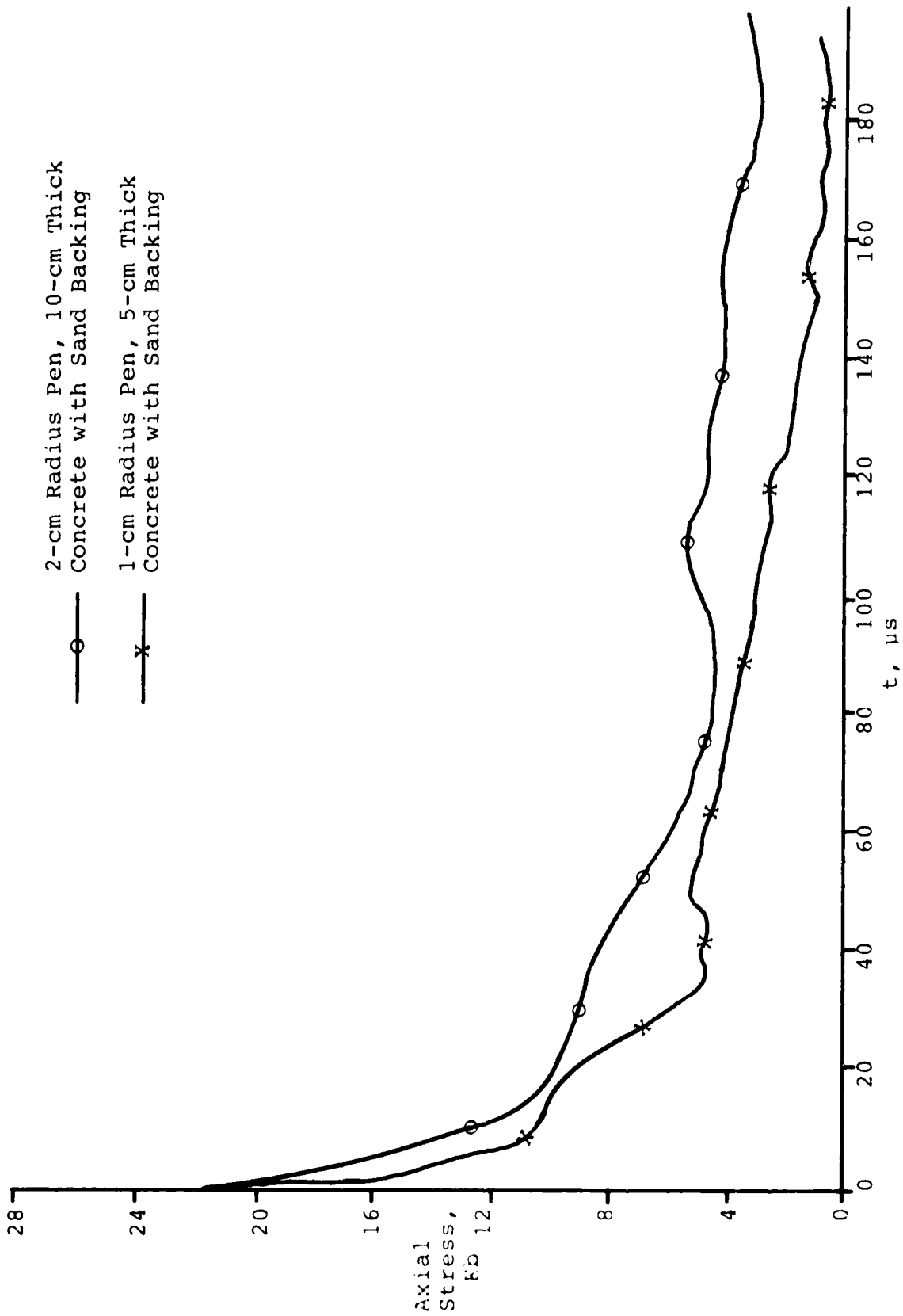
Figure 26. Blunt Projectiles at T/D=5 and V=300 m/s.

2-cm Radius Pen, 10-cm Thick Concrete with Sand Backing

1-cm Radius Pen, 5-cm Thick Concrete with Sand Backing

Axial Stress, KB

t, µs

38
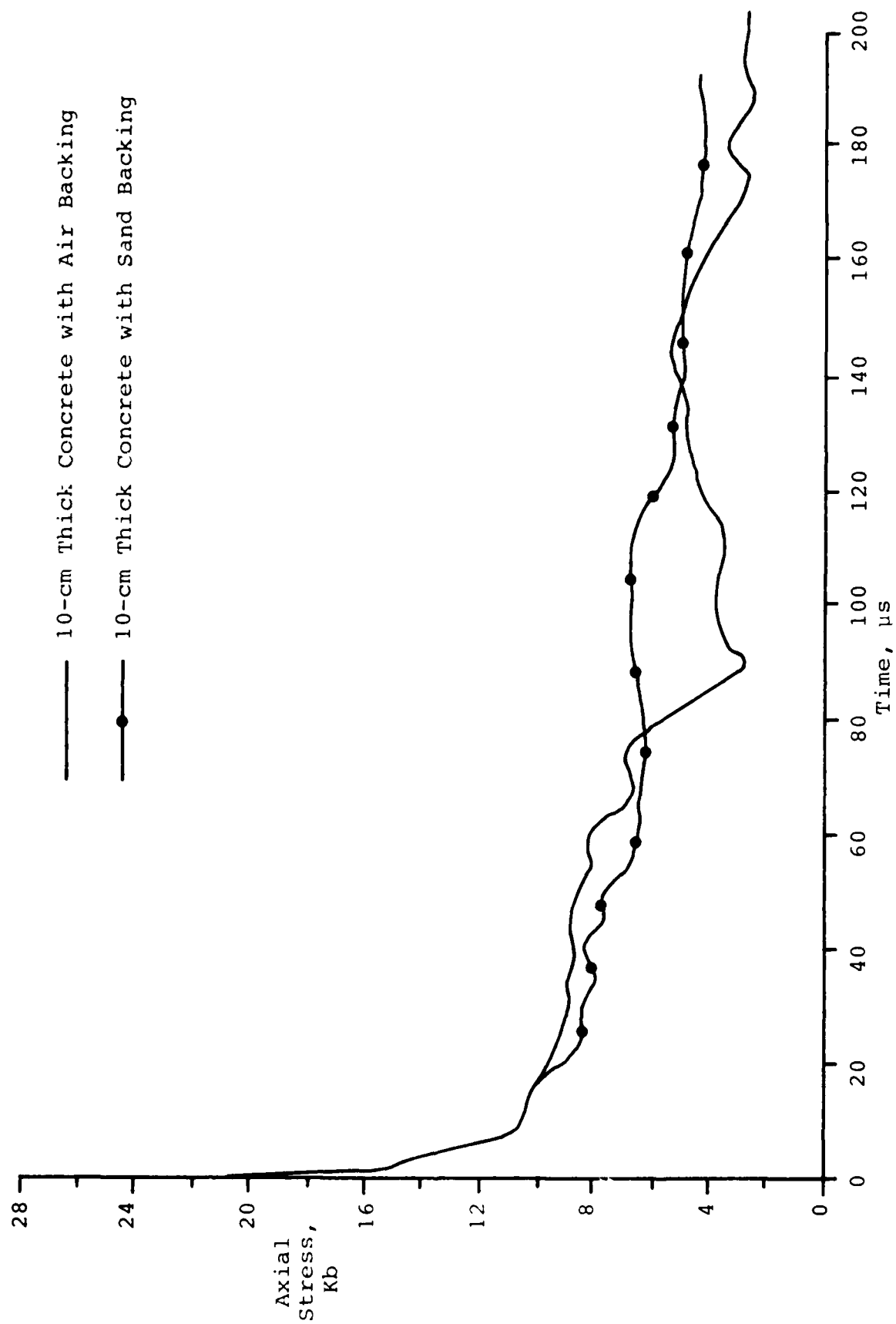
Figure 27. 1-cm Radius Projectiles at 300 m/s.

39
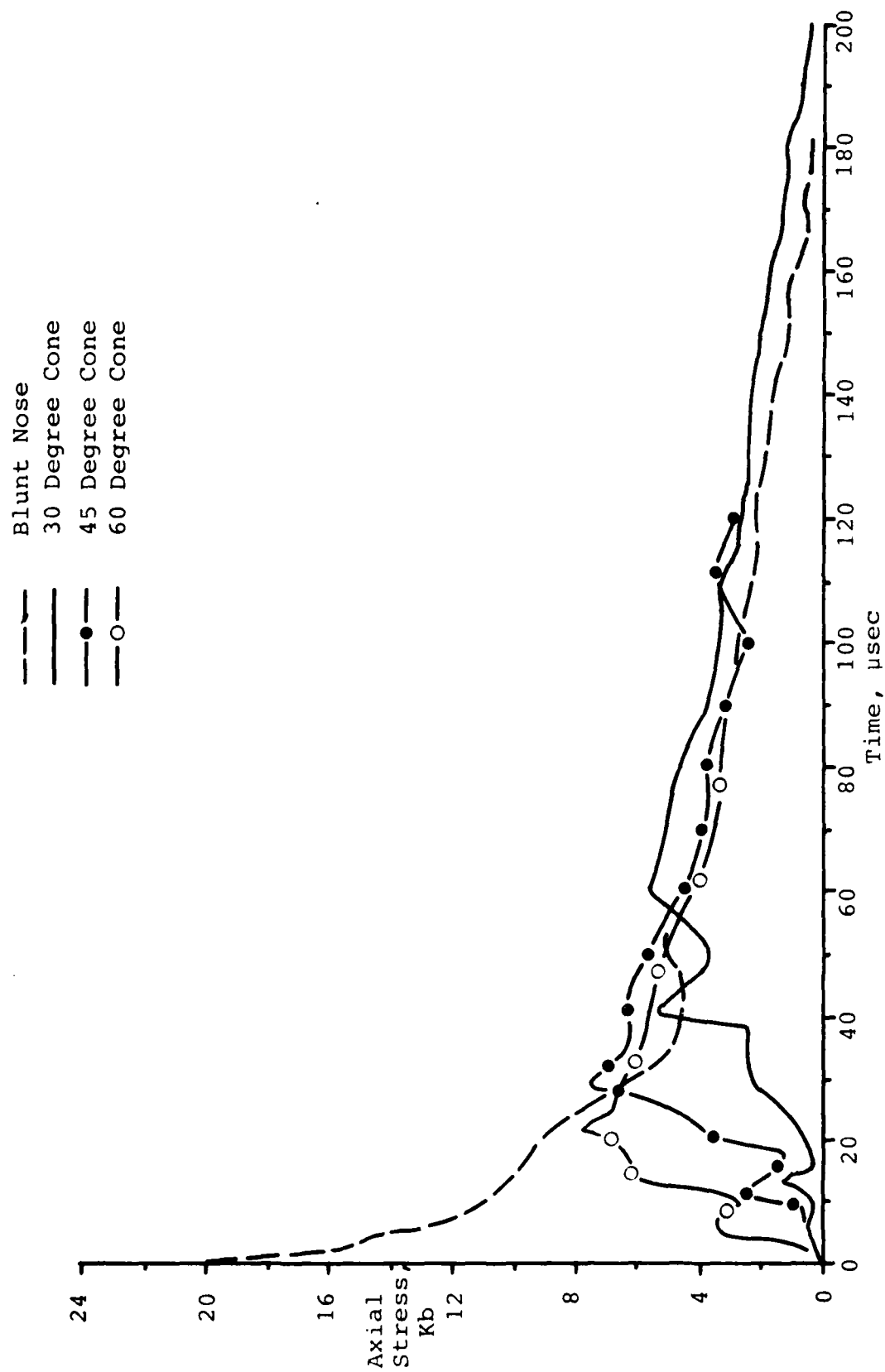
Figure 28. 1-cm Radius Projectiles at 300 m/s Into 5-cm Concrete/Sand.

40

dividing applied force by the largest cross-sectional area of the projectile. For a conically-nosed projectile, this results in lower initial stress until the complete cone is buried in the concrete. The stress levels would be similar to those seen in the blunt projectile if the actual 'wetted' areas had been employed.

Figure 29 compares a blunt and a 45-degree conically-nosed projectile at 300 m/s into a sand-backed concrete slab 10-cm thick. For this thickness, the blunt projectile sees slightly higher loading after the nose of the cone is buried in the concrete. Still, the loading is reasonably close after this point.

Figure 29. Loading for 1-cm Radius Projectiles Into 10-cm Thick Concrete With Sand Backing at 300 m/s.

42

SECTION IV
THE LOADING MODEL

There are a number of possible methods which could be used to construct a model for projectile or projectile element loading. Differences in methods used will not be important if the major parameters are represented in the model. Calculations presented in the previous section indicate that velocity, V, concrete slab thickness, T, projectile or element diameter, D, are the major parameters needed to determine stress versus time loadi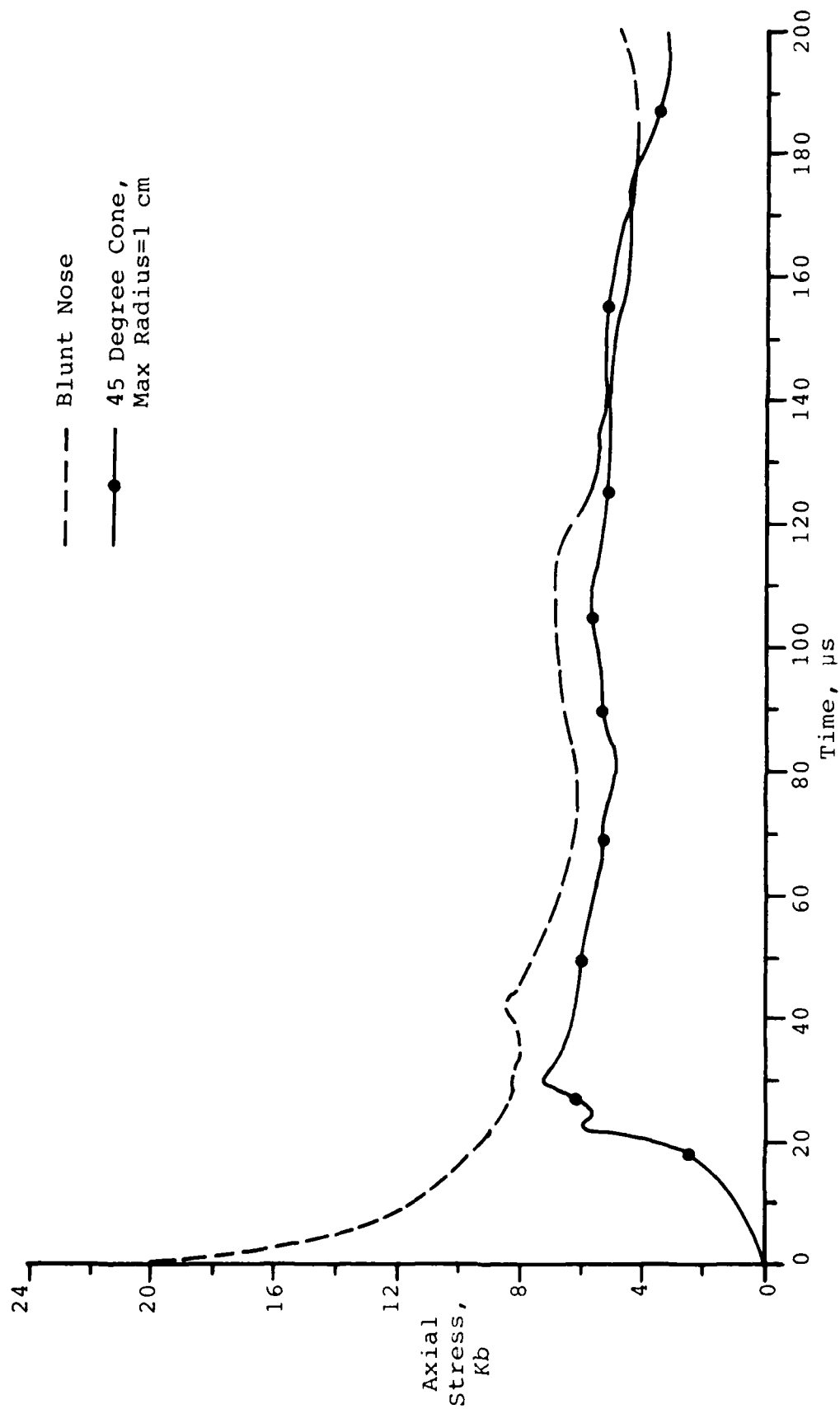ng curves. Using these parameters, a simple model will be constructed for blunt projectiles or elements with a surface oriented normally to the flow. Later in the section, modifications required for other than normal surface orientation will be discussed.

It seems reasonable to model loading as a modification to the semi-infinite loading model. Examination of the many calculations leads to a simple loading curve as seen in Figure 30 for blunt projectiles at a given T/D and a velocity greater than 300 m/s. Based on the calculations, changes from the semi-infinite model of Reference 1 are not recommended for velocities below 300 m/s. In this curve, τ is the axial stress on the projectile or projectile element. Point 1 on the curve is the peak stress generated within a few microseconds after impact. This stress is a function of velocity only and is plotted, along with the point 2 stress level in Figure 31. The peak is used for point 1 stress and the steady value for point 2. The peak curve is closely fit with the expression:

$$\tau_1 = \rho c V$$

where ρ is 2.2 gm/cc, c is 3.1×10^5 cm/s and V is the projectile's velocity in cm/s. The result is peak stress in dynes/cm^2 (to convert to Kb, divide by 10^9). The sound speed in this equation is a few percent larger than that recommended in Reference 1. The steady stress level is fit with the expression:
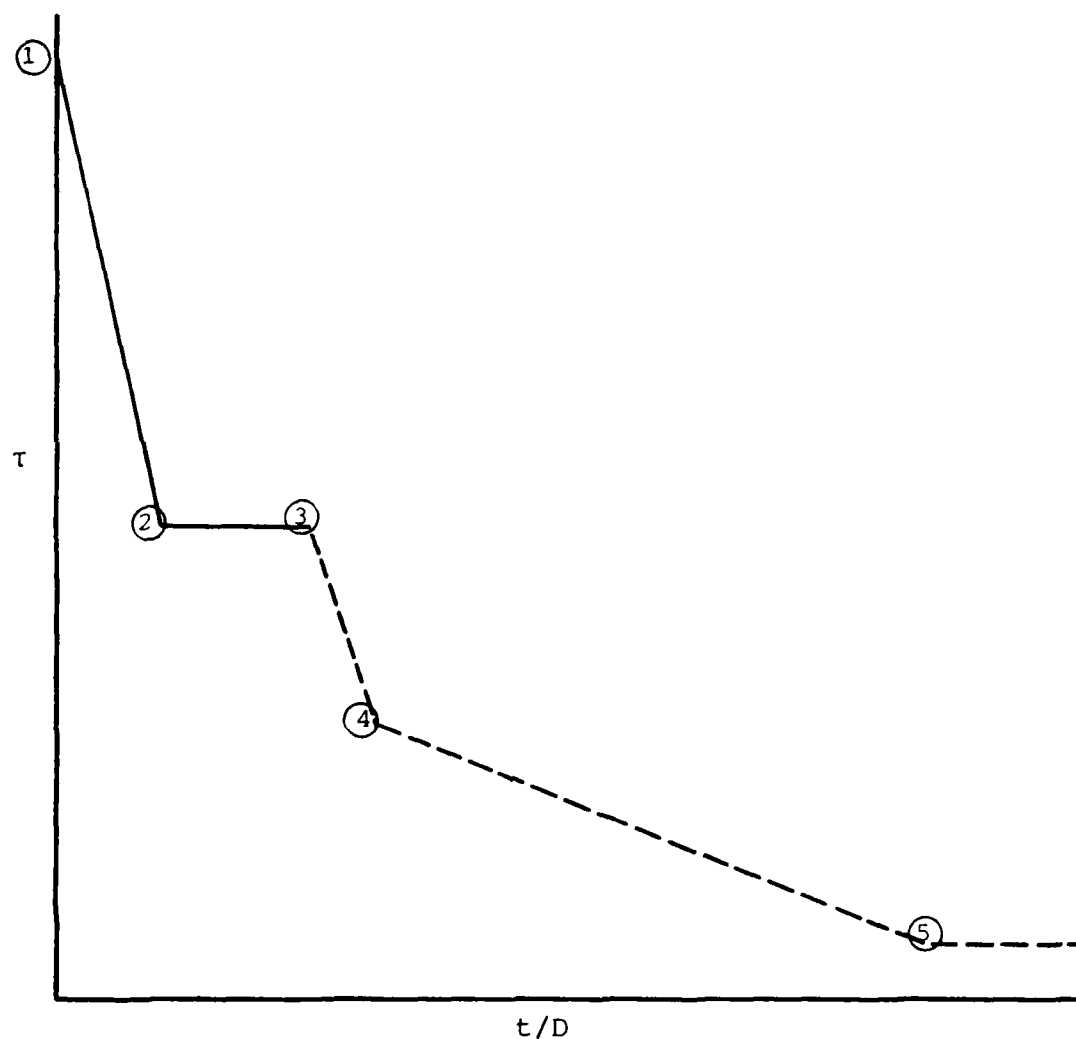
$$\tau_2 = \tau_3 = 0.6 \ \rho c V$$

Figure 30. Loading Curve for Blunt Projectiles for
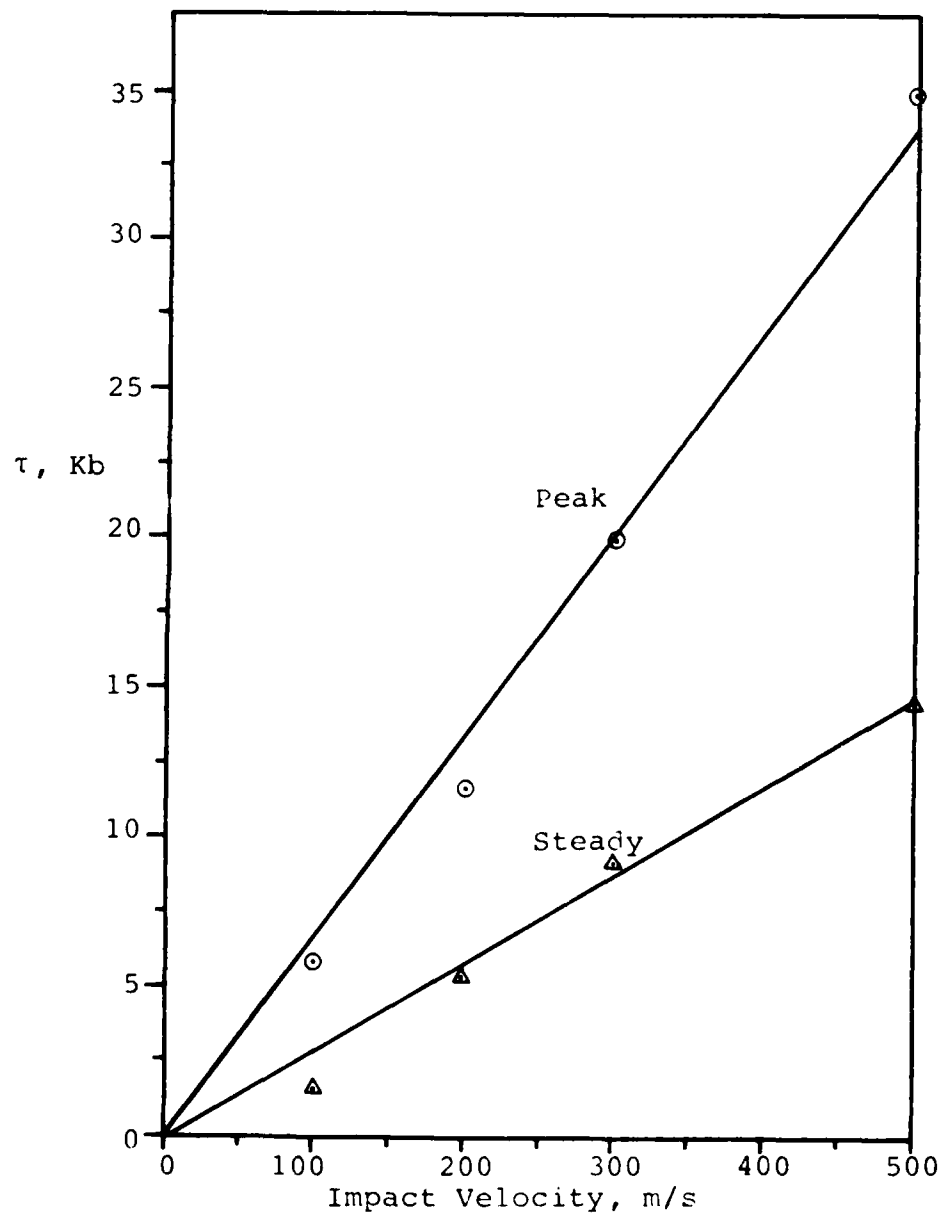a Specific Velocity and T/D.

44

Figure 31. Peak and Steady Stress Levels Versus
            Velocity.

where ρ is 2.2 gm/cc, c is 2.27×10^5 cm/s and V is in cm/s. The value of c is very close to that recommended in Reference 1. It is believed to provide a slightly better fit to the calculations. The factor of 0.6 is explained in Reference 1 and results from the flow field moving radially away from the projectile at the time the steady stress level is achieved.

The scaled time (t/D) at which point 2 is reached is given in Reference 1 as:

$$(t/D)_2 = 14 \times 10^{-6} \text{ s/cm}$$

Data in the calculations in this report support that fit as valid and it will be used to describe point 2.

Point 3 is the point in time at which returns from the concrete interface begin to significantly affect loading. Figure 32 shows data from the calculations at 300 and 500 m/s (the velocities at which loading was significantly affected). There is some uncertainty in the value of $(t/D)_3$ for a 10-cm thick concrete and 500 m/s velocity. The bar indicates the range of uncertainty. It was decided to use the point at 20×10^{-6} s/cm because it fits the 300 m/s data and because that is really the point at which stress begins to diverge most radically from the semi-infinite case at 500 m/s. Using this fit, the equation for $(t/D)_3$ becomes:

$$(t/D)_3 = 4(T/D) \times 10^{-6} \text{ s/cm}$$

Point 4 on the loading curve is somewhat of an idealization in that it does not take into account the sharp drop caused by return of the peak loading stress from the sand or air interface. It was decided to ignore this peak return because of its short-lived nature. Stress and scaled time data for point 4 were selected from the 300 and 500 m/s loading curves and are seen in Figures 33 and 34. These figures indicate that τ_4, the stress at point 4, should be a function of velocity as well as T/D. In the range of 300 to 500 m/s, a good fit for τ_4 appears to be:

$$\tau_4 = 2 + (6/5)T/D + 3(V-3 \times 10^4)/2 \times 10^4$$
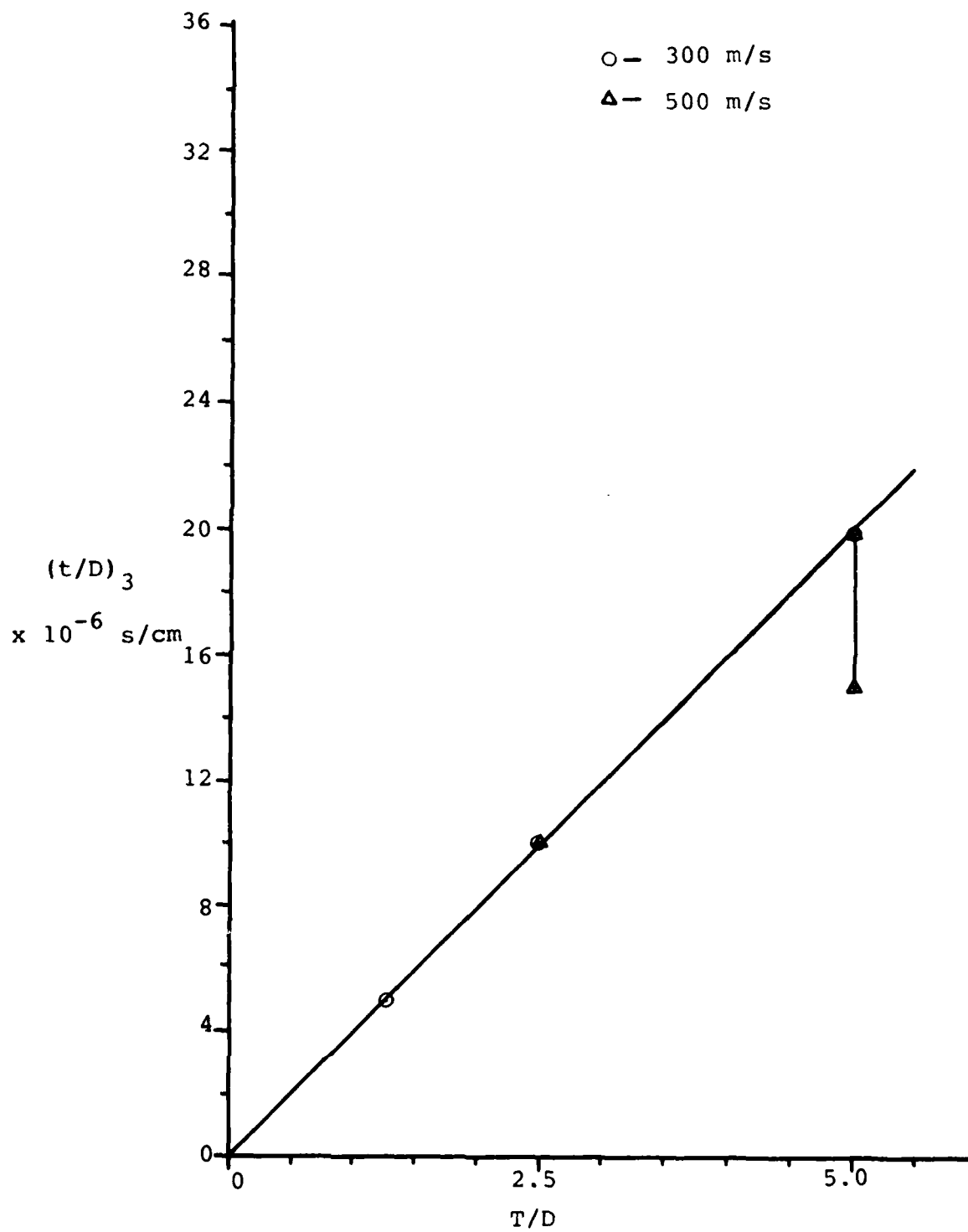
where τ_4 is in kilobars and V is in cm/s.

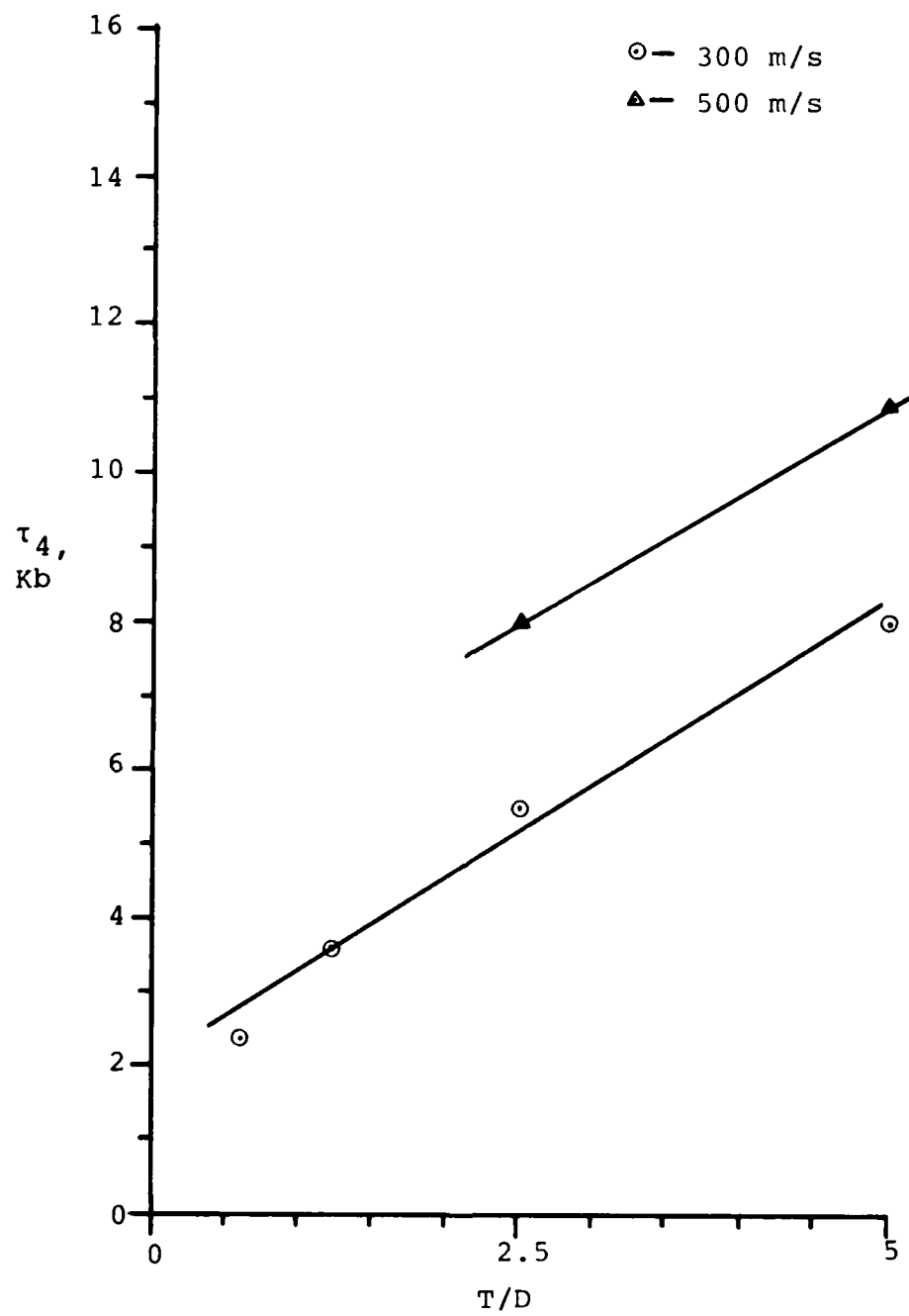Figure 32. $(t/D)_3$ Versus T/D for 300 and 500 m/s.
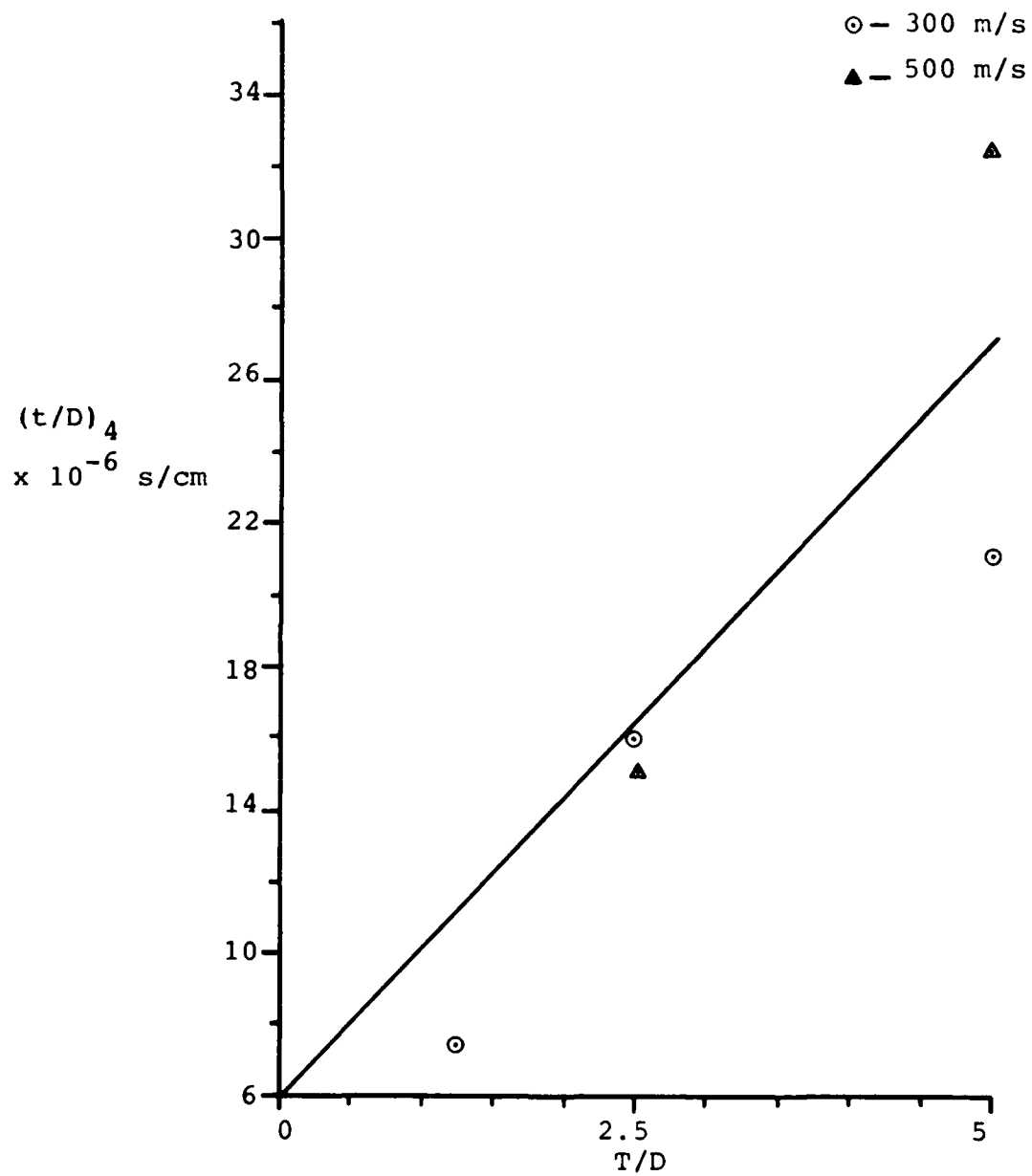
Figure 33. τ_4 Versus T/D.

Figure 34. $(t/D)_4$ Versus T/D for Blunt Projectiles.

49

Calculational data for the scaled time, $(t/D)_4$, is seen in Figure 34. The data do not lie too far from a single straight line, expressed by:

$$(t/D)_4 = 5.4 \times 10^{-6} (T/D) \text{ s/cm}$$

The final stress level, τ_5, has some uncertainty surrounding it because there were not many calculations carried to this late time. It appears, however, that use of the equation:

$$\tau_5 = 1/2 \rho V^2 \times 10^{-9}$$

where V is in cm/s and τ_5 is in Kb, is adequate and reasonably fits the data available.

Figure 35 plots the data available for the scaled time, $(t/D)_5$. This scaled time is a function of T/D and velocity. A fit to this data is as follows:

$$(t/D)_5 = \left\{ 32 - 13 \left(\frac{V - 3 \times 10^4}{2 \times 10^4} \right) (T/D) \right\} \times 10^{-6} \text{ s/cm}$$

where V is in cm/s.

The model, then, for blunt projectiles or projectile elements is the curve described in Figure 30 with τ_i and $(t/D)_i$ fits as expressed in the previous equations.

This blunt projectile model appears to be adequate for cones or projectile elements with non-zero yaw if the actual wetted area is used for force development. If the entire element or projectile area is used, then one must intersect the blunt loading curve at a time at which the entire element or nose section becomes wetted. A straight line from $\tau=0$ to an intersection at completely wetted time fits the calculations.
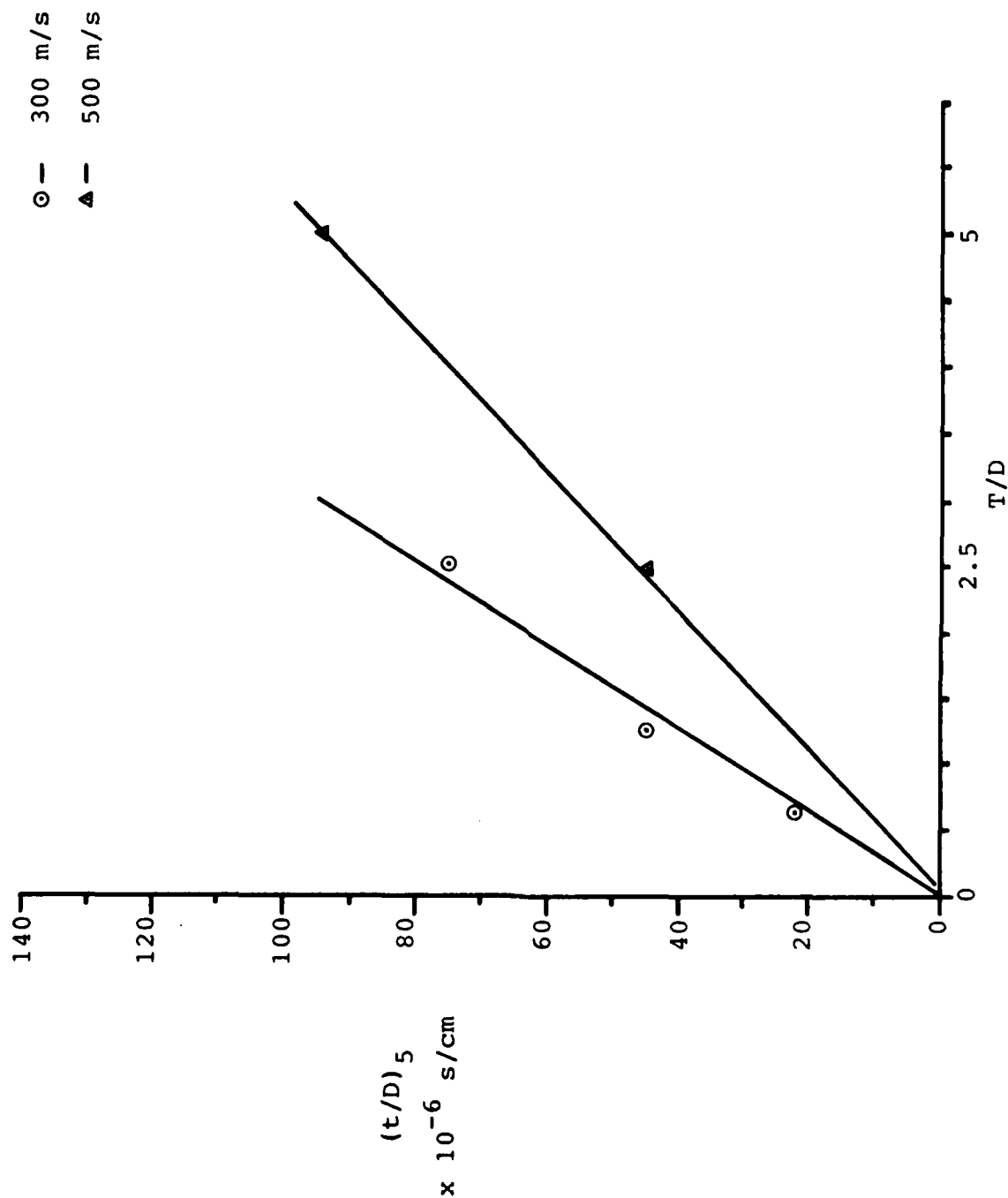
Figure 35. $(t/D)_5$ Versus T/D for Blunt Projectiles.

51

SECTION V

EFFECTS OF SATURATED CONCRETE

Two calculations were run investigating the effect of saturated concrete on expected loading. The projectile was a blunt, 1-cm radius vehicle travelling at 300 m/s.

In the first calculation, the projectile impacted a semi-infinite slab of fully saturated concrete. The loading curve resulting from this calculation is seen in Figure 36. Also seen in the figure is the loading expected upon impact into the same slab of dry concrete. The calculation indicates that initial peak stress is higher in the saturated concrete but that the steady stress value is essentially $(1/2)\rho V^2$, or that expected from merely pushing failed concrete. Examination of the calculation shows that the high speed of relief waves from the entrance-free surface accounts for the rapid reduction of loading on the projectile.

The existence of sand in front of the concrete has little effect, as seen in Figure 37. This figure presents loading on a 1-cm radius projectile impacting saturated concrete covered with a 10-cm thick layer of sand. Loading experienced by the projectile in the concrete is close to that seen in Figure 37 after peak stresses have decayed.

These calculations indicate that a saturated concrete which obeys Hightower's behavior model is a very soft target.
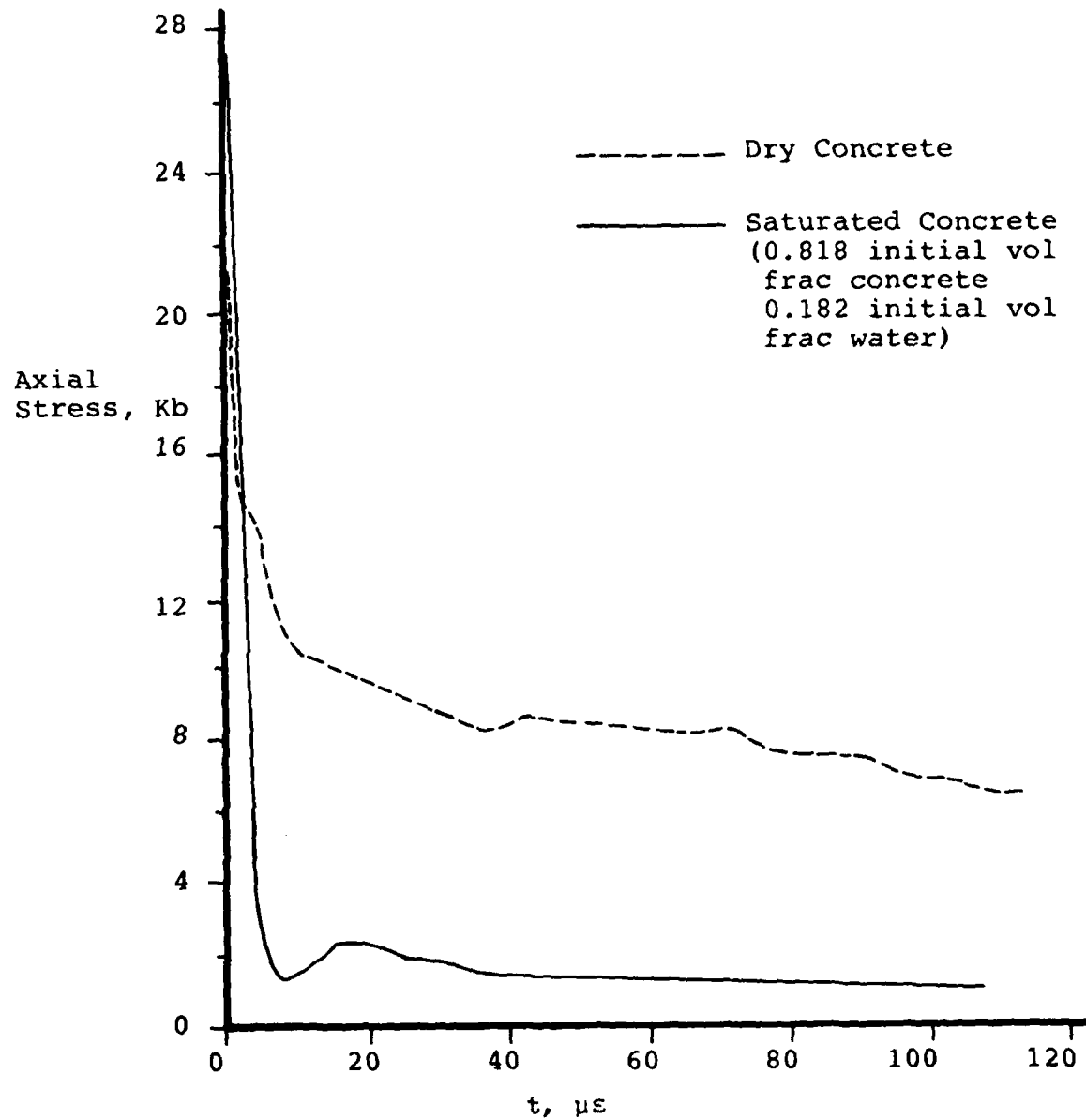
Figure 36. Loading on 1-cm Radius Blunt Penetrator
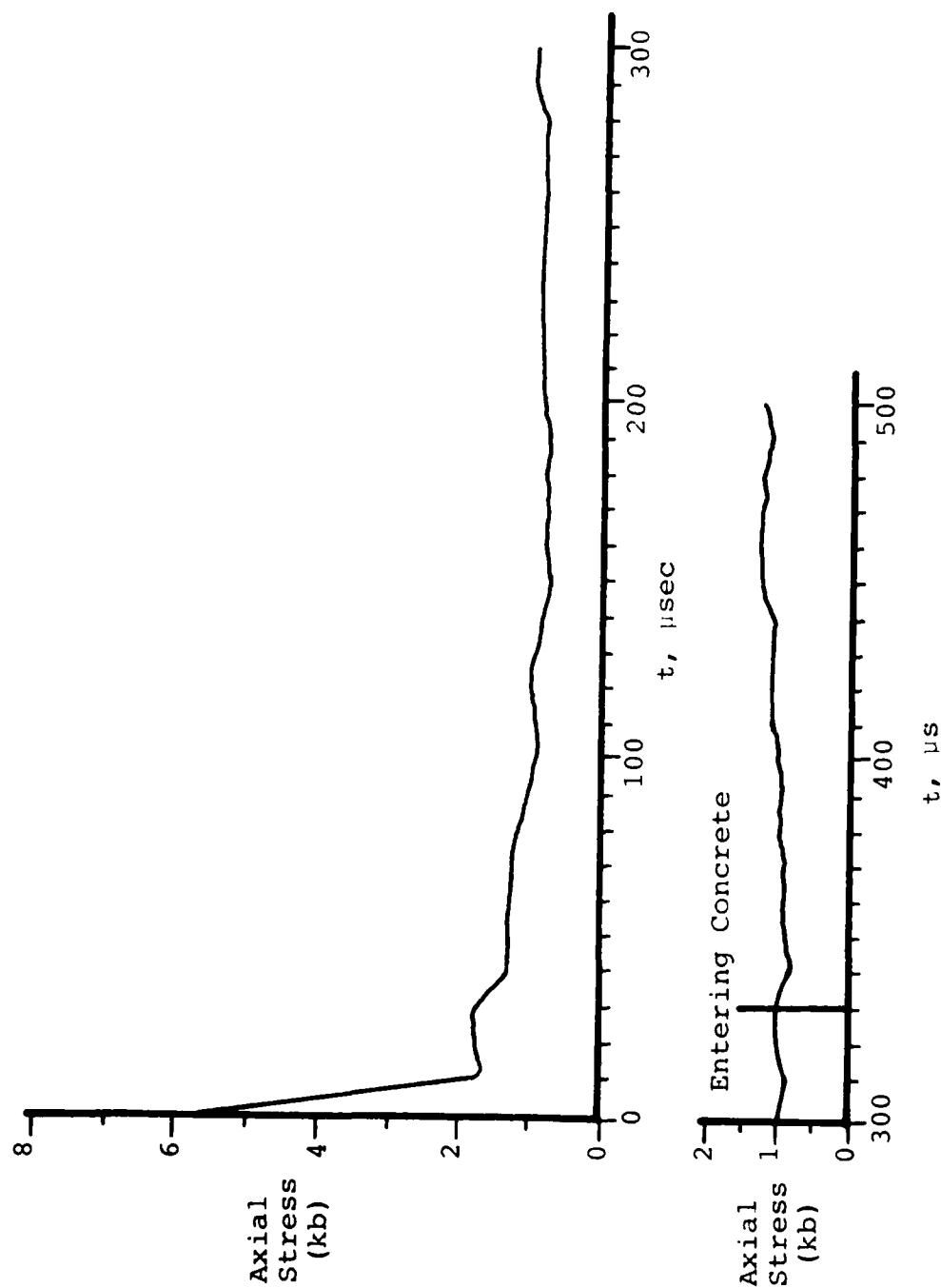Impacting Concrete at 300 m/s.

53

Figure 37. Loading on 1-cm Radius Blunt Penetrator at 300 m/s in 10-cm Sand Over Saturated Concrete.

54

SECTION VI
RECOMMENDED EXPERIMENTAL EVALUATION

The work described in this report extends the concrete loading model developed for semi-infinite targets to targets with finite thickness both with and without sand backing. Expressions are developed for the initial impact stress loading on the projectile and for the steady state loading. The appropriate expressions are linear fits to calculated data and the inflection points are related to a scaled time which is proportional to the T/D ratio of the concrete/projectile system.

Using a suitable transducer and an on-board recording system, it should be possible to measure the axial stress loading on the nose of a penetrating projectile and assess the overall qualitative and quantitative agreement between the calculations and experiment. At impact velocities of 220 m/sec or less, the steady state loading stress will be less than the maximum allowable for existing ballistic pressure transducers (~6.2 Kbar). By providing for a recessed installation to eliminate the initial impact stress on the transducer, and by suitable conditioning of the output signal, it is likely that an accurate dynamic recording of the steady state stress can be obtained. The use of different target thicknesses along with a single projectile diameter will provide suitable verification of the scaled time relationship for unloading times in the finite thickness targets. A limited series of 6 tests will be suitable for initial verification of the loading curve. If the technique adopted proves feasible, then it could be further extended to oblique impact cases with either axial or radial stress measurements. Data developed from such a program may be employed along with plane strain calculations to extend the utility of the loading model to oblique impact situations, as appropriate.

Current interest in projectile ricochet from concrete surfaces combined with a general lack of experimental data to evaluate proposed ricochet criteria points to the need for a testing program to develop suitable information. Many experimental efforts involving ricochet are performed with subscale projectiles such as 0.50 caliber or 20 mm in order to minimize projec-

55

tile costs, to ease data collection requirements and to permit a relatively large number of tests to be conducted. The typical problem associated with such subscale testing is that the concrete target and projectiles are not replica models of full scale items of interest, and the data developed has limited utility. Full scale testing usually is expensive, and consequently, only limited tests are performed to satisfy a particular developmental requirement. This is particularly so for items launched full scale from a rocket sled track. A compromise approach which employs relatively large projectiles of about 8 cm diameter is possible using a smooth bore gun developed by the Air Force Armament Laboratory at Eglin Air Force Base. Such a system would tend to minimize the problems of scaling test results since for many systems, the results are very nearly full scale. In addition, overall expense would be less than 10 percent of a comparable program using very large targets on a sled track.

Based upon a nominal projectile diameter of 8 cm, a test program requiring approximately 36 tests would be appropriate to evaluate ricochet from targets of 3 different thicknesses at 2 different velocities, at 3 angles of obliquity and with 2 different nose shapes. With target thicknesses of 4, 12 and 36 inches, target thickness to projectile diameter ratios of from 1.3 to 11.4 should be investigated at the different velocities. The loading model developed in this report indicates that loading—and hence, ricochet—is a strong function of the projectile diameter to target thickness ratio. Targets need to be well characterized with compressive cylinder tests and beam flexure tests and should be 8 feet square to minimize edge effects. By employing high speed cameras and witness panels, the entry and exit trajectories could be accurately determined and the data used for comparisons with calculation made from the Differential Area Force Law (DAFL) code and/or the Terradynamic Equations of Motion (TDEM) code both currently used by the Armament Laboratory. The overall series should provide a comprehensive set of data suitable for use in verifying existing ricochet predictors.

56

REFERENCES

1. Osborn, J. J., 'A Preliminary Model for Loads on a Penetrator Impacting Concrete', AFATL TR 81-53, ARBRL-CR-00456, June 1981.

2. Osborn, J. J. and Matuska, D. A., 'Dynamic Response of a Kinetic Energy Penetrator', AFATL TR-78-24, Vol II, March 1978.

3. Hightower, M. M., 'Theoretical and Experimental Constitutive Relations of Concrete', Sandia National Laboratories, April 1981.

4. Allen, Mayfield and Morrison, J. Appl. Phys., 28, 1957.

5. Van Thiel, 'Compendium of Shock Wave Data', UCRL-50108, Rev 1, Lawrence Livermore National Laboratory, June 1977.

6. Swegle, J. W., 'TOODY IV - A Computer Program for Two-Dimensional Wave Propagation', Sandia Report SAND-78-0552, Sep 78.

7. Durrett, R. E. and Matuska, D. A., 'The HULL Code, Finite Difference Solution to the Equations of Continuum Mechanics', AFATL TR-78-125, Nov 78.

(The reverse of this page is blank)